Protein tyrosine phosphatase receptor type R (PTPRR) antagonizes the Wnt signaling pathway in ovarian cancer by dephosphorylating and inactivating β-catenin

Received for publication, August 1, 2019, and in revised form, October 15, 2019 Published, Papers in Press, October 25, 2019, DOI 10.1074/jbc.RA119.010348

Yuetong Wang[‡1], Jian Cao[§1], Weiwei Liu[¶1], Jiali Zhang[‡], Zuo Wang[‡], Yiqun Zhang[¶], Linjun Hou[‡], Shengmiao Chen[‡], Piliang Hao[‡], Liye Zhang[‡], Min Zhuang[‡], Yang Yu[¶], Dake Li[§2], and Gaofeng Fan[‡3]

From the [‡]School of Life Science and Technology, ShanghaiTech University, Shanghai 201210, China, the [§]Department of Gynecology, Women's Hospital of Nanjing Medical University, Nanjing Maternity and Child Health Care Hospital, Nanjing 210004, China, the [¶]Institute of Biophysics, Key Laboratory of RNA Biology, Chinese Academy of Sciences, University of Chinese Academy of Sciences, Beijing 100101, China

Edited by Eric R. Fearon

Despite a lack of mutations, accumulating evidence supports an important role for the Wnt/β-catenin pathway in ovarian tumorigenesis. However, the molecular mechanism that contributes to the aberrant activation of the Wnt signaling cascade in ovarian cancer has not been fully elucidated. Here, we found that protein tyrosine phosphatase receptor type R (PTPRR) suppressed the activation of the Wnt/β-catenin pathway in ovarian cancer. We performed an shRNA-based biochemical screen, which identified PTPRR as being responsible for tyrosine dephosphorylation of β-catenin on Tyr-142, a key site controlling the transcriptional activity of β-catenin. Of note, PTPRR was down-regulated in ovarian cancers, and ectopic PTPRR re-expression delayed ovarian cancer cell growth both *in vitro* and *in vivo*. Using a proximity-based tagging system and RNA-Seq analysis, we identified a signaling nexus that includes PTPRR, α-catenin, β-catenin, E-cadherin, and AT-rich interaction domain 3C (ARID3C) in ovarian cancer. Immunohistochemistry staining of human samples further suggested that PTPRR expression is inversely correlated with disease prognosis. Collectively, our findings indicate that PTPRR functions as a tumor suppressor in ovarian cancer by dephosphorylating and inactivating β-catenin. These results suggest that PTPRR expression might have utility as a prognostic marker for predicting overall survival.

Ovarian cancer is one of the deadliest malignant tumors and the fifth-leading cause of cancer-related death in women from the United States (1, 2). Over the last 2 decades, advances have greatly improved cancer therapy; however, the survival rate of women with ovarian cancer has barely changed (3–5). Thus, further research is needed to understand how different molecular pathways contribute to tumorigenesis of ovarian cancer and to discover potential therapeutic targets.

The Wnt signaling pathway comprises a large family of glycoproteins known mostly for their critical function in embryonic development, including cell fate determination, differentiation, proliferation, and apoptosis (6, 7). As a result, mutations in the Wnt pathway are often linked to birth defects, cancer, and other diseases in humans (7). Several reports have shown that Wnt/β-catenin signaling is frequently dysregulated in ovarian cancers (8–10). In a comprehensive analysis of 47 primary ovarian specimens, the Wnt/β-catenin pathway was defective in nearly half of the samples (11). The key signaling molecule of the canonical pathway, β-catenin, is often mutated in endometrioid ovarian carcinomas (12–14). In serous, clear cell, and mucinous ovarian carcinomas, although gene mutations in the Wnt/β-catenin pathway are rare, hyperactivation of the pathway and β-catenin–targeted genes are still required for ovarian cancer development (10, 15–17). Therefore, the Wnt pathway is investigated as a potential target in the treatment of ovarian cancer, and the molecular mechanisms of aberrant activation in ovarian cancer should be further studied.

Among multiple tiers of regulation, tyrosine phosphorylation plays an important role in controlling the function of β-catenin (18). Two tyrosine residues in β-catenin are the center of this regulation: tyrosine 142 and 654. SRC, Fyn, and FER kinases are responsible for phosphorylating these sites. Upon phosphorylation, the E-cadherin–β-catenin–α-catenin complex collapses at the plasma membrane, and the released β-catenin translocates to the nucleus for its function as a transcriptional factor (19–23). Tyrosine 654 is indispensable for association with E-cadherin (19, 23). More importantly, the phosphorylation status of Tyr-142 of β-catenin determines the switch between the adhesive and the transcriptional functions of β-catenin. α-Catenin and nuclear factor BCL9-2 share an overlapping binding site on β-catenin, which includes the first armadillo repeat, where Tyr-142 resides (22, 24). Either tyrosine phosphorylation or a mutation to glutamic acid, which

This work was supported by Ministry of Science and Technology of China Grant 2018YFC1004603 (to G. F.), National Natural Science Foundation of China Grant 31872831 (to G. F.), Shanghai Pujiang Program Grant 18PJ1407900 (to G. F.), and ShanghaiTech University Startup Grant F-0202-17-041 (to G. F.). The authors declare that they have no conflicts of interest with the contents of this article.

This article contains Tables S1 and S2 and Figs. S1–S3.

The mass spectrometry proteomics data have been deposited to the ProteomeXchange Consortium via the PRIDE (57) partner repository with the data set identifier PXD015352.

The RNA-Seq raw data have been deposited in GEO, and the project ID is GSE135220.

[1] These authors contributed equally to this work.
[2] To whom correspondence may be addressed. E-mail: lidake2002@163.com.
[3] To whom correspondence may be addressed. E-mail: fangf@shanghaitech.edu.cn.

increases a negative charge on residue 142 in β-catenin, promotes binding to BCL9-2 over α-catenin (24). This BCL9-2 binding stabilizes the phosphorylation of β-catenin and facilitates its nuclear translocation and further binding with LEF/TCF proteins, resulting in increased transcription of Wnt/β-catenin target genes (24, 25). Phosphorylation of Tyr-142 of β-catenin thus becomes a reliable marker to illustrate the activation of Wnt/β-catenin signaling and assess the consequences of perturbing this pathway to human disease.

In the current study, using a shRNA-based biochemical screen, we determined that protein tyrosine phosphatase PTPRR,[4] which is down-regulated in ovarian cancers, is responsible for tyrosine dephosphorylation of β-catenin on residue 142. Ectopic expression of PTPRR decreases tyrosine phosphorylation of β-catenin, inhibits the β-catenin–mediated transcriptional activation of downstream target genes, and significantly delays ovarian cancer cell proliferation both *in vitro* and *in vivo*. Overall, we reported a negative regulatory function of PTPRR in ovarian cancer oncogenesis, and the expression level of the phosphatase could be a good prognostic marker for overall survival of patients.

Results

Aberrant activation of the Wnt/β-catenin pathway in ovarian tumors and ovarian tumor–derived cell lines

Hyperactivation of β-catenin–mediated Wnt signaling is a major contributing factor of ovarian tumorigenesis (17, 26). Phosphorylation of tyrosine 142 of β-catenin provides a feasible marker to quickly screen the activation status of pathways in ovarian cancers, so we used specific pTyr-142 antibody against β-catenin for immunohistochemistry analysis of tissue array including 133 cases of serous carcinoma, 34 mucinous adenocarcinoma, 3 adenocarcinoma, 7 endometrioid adenocarcinoma, 15 metastatic carcinoma, and 8 adjacent normal ovary tissue. Whereas both adjacent normal ovary tissue and ovarian tumor samples showed equivalent expression levels of total β-catenin, the Tyr-142 phosphorylation signal in tumor samples was significantly higher than normal control (Fig. 1, *A* and *B*). In total, 192 ovarian tumor samples were assessed: 20 of the samples were pTyr-142 and β-catenin double-negative; 42 samples were β-catenin–positive but pTyr-142–negative; and 130 of the samples were pTyr-142 and β-catenin double-positive (Fig. 1*B*). The ratio of pTyr-142 β-catenin–positive samples was higher in tumor patients than in adjacent normal controls (Fig. 1*B*). Moreover, the ratio of pTyr-142 β-catenin–positive tumor samples was increased with grading advancement of the disease (Fig. 1*C*). However, a similar trend was not observed in terms of the stage of tumor samples (Fig. 1*D*). The International Federation of Gynecology and Obstetrics (FIGO) stage is classified according to the TNM Classification of Malignant Tumors, which was closely related to the tumor metastasis states. The tumor grade generally refers to the degree of differentiation or maturity of the cells that make up the tumor within the ovarian primary tumors. Because we analyzed the primary tumor samples, we thought that the tumor grade was more relevant than tumor stage in our scenario.

In addition, we did immunoblotting analysis to compare phosphorylation level of Tyr-142 β-catenin in both ovarian tumor samples from patient and normal ovarian tissue control. Four of eight tumor samples showed evidently high pTyr-142 β-catenin level, whereas all six normal ovarian tissues showed trace amounts of pTyr-142 β-catenin (Fig. 1*E*).

To further evaluate the activation status of the Wnt/β-catenin pathway in ovarian tumors, we compared the distribution of β-catenin in 11 ovarian tumor-derived cell lines with two human ovarian surface epithelial (HOSE) cell lines immortalized by the human papilloma viral oncogenes E6 and E7 as a negative control (27). Sequences of β-catenin from these cell lines were examined before the experiment, and no mutations were detected. We observed a significant increase of nuclear β-catenin in most ovarian cancer cells examined (Fig. 1*F*). Consistently, phosphorylation of β-catenin on Tyr-142 was also enhanced in these tumor-derived cell lines (Fig. 1*G*). Moreover, several co-activators of β-catenin, including LEF1, TCF1, TCF3, and TCF4, were selectively up-regulated in most ovarian cancer-derived cell lines, whereas Wnt signaling antagonist SFRP1 was underexpressed compared with normal controls (Fig. 1*G*).

We also adopted the TOP/FOP reporter system to further confirm Wnt signaling activation in ovarian cancer cell lines. As shown in Fig. 1*H*, the intensity of TOP luciferase was significantly higher in PA-1, CAOV4, and OVCAR5 compared with HOSE cell lines. Collectively, all of this evidence suggested aberrant activation of the Wnt/β-catenin pathway during the oncogenesis of ovarian cancer.

A protein tyrosine phosphatase screen identified PTPRR as one of the major tyrosine phosphatases responsible for dephosphorylation of β-catenin at Tyr-142

We and others have reported previously that the protein tyrosine kinase FER is a key regulator of Tyr-142 phosphorylation of β-catenin (28, 29). Furthermore, other kinases, including SRC, have also been suggested to modulate this phosphorylation event under different stimulation conditions (19). By using phosphotyrosine antibody, several PTPs have been identified as β-catenin phosphatases (30). Given that multiple tyrosine residues within the β-catenin sequence could be phosphorylated upon stimulation, these findings could not reveal which phosphatase is responsible for dephosphorylation of β-catenin at Tyr-142.

In an initial attempt to address this question, we infected MCF10A cells with shRNA against each individual classical protein tyrosine phosphatase (37 in total) and selected stable cell lines with consistent expression of the designated shRNA. The reasons we use normal breast cells (MCF10A) for screening purpose are as follows: 1) we prefer to use normal cell lines rather than cancer cells, because some genes, like protein tyrosine phosphatases, are usually silenced in cancers; 2) we chose

[4] The abbreviations used are: PTPRR, protein tyrosine phosphatase receptor type R; FIGO, International Federation of Gynecology and Obstetrics; HOSE, human ovarian surface epithelial; FBS, fetal bovine serum; EGF, epidermal growth factor; qRT-PCR, quantitative RT-PCR; PUP-IT, pupylation-based interaction tagging; ARID3C, AT-rich interaction domain 3C; CTG, Cell Titer-Glo; ERK, extracellular signal-regulated kinase; HCD, higher-energy collisional dissociation; FDR, false discovery rate; TBS, Tris-buffered saline; IHC, immunohistochemistry.

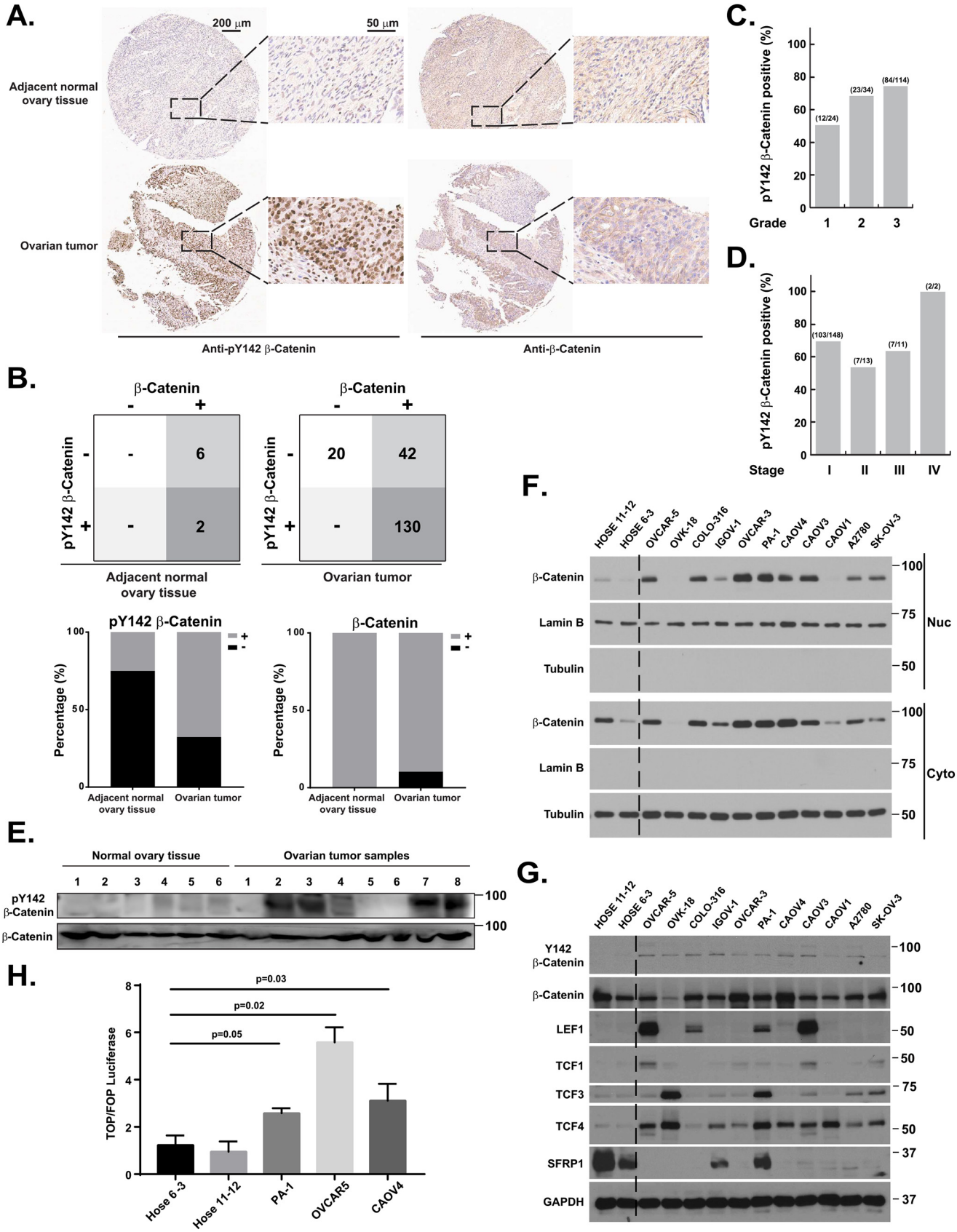
A.
200 μm
50 μm
Adjacent normal ovary tissue
Ovarian tumor
Anti-pY142 β-Catenin
Anti-β-Catenin
B.
β-Catenin
pY142 β-Catenin
6
2
20
42
130
Adjacent normal ovary tissue
Ovarian tumor
pY142 β-Catenin
β-Catenin
Percentage (%)
C.
pY142 β-Catenin positive (%)
(12/24)
(23/34)
(84/114)
Grade
D.
pY142 β-Catenin positive (%)
(103/148)
(7/13)
(7/11)
(2/2)
Stage
I
II
III
IV
E.
Normal ovary tissue
Ovarian tumor samples
pY142 β-Catenin
β-Catenin
F.
HOSE 11-12
HOSE 6-3
OVCAR-5
OVK-18
COLO-316
IGOV-1
OVCAR-3
PA-1
CAOV4
CAOV3
CAOV1
A2780
SK-OV-3
β-Catenin
Lamin B
Tubulin
Nuc
Cyto
G.
Y142 β-Catenin
β-Catenin
LEF1
TCF1
TCF3
TCF4
SFRP1
GAPDH
H.
p=0.03
p=0.02
p=0.05
TOP/FOP Luciferase
Hose 6-3
Hose 11-12
PA-1
OVCAR5
CAOV4

MCF10A rather than normal ovarian control HOSE11-12 and HOSE6-3, because both of these ovarian cell lines are very difficult to subject to infection procedures to make stable cell lines for further investigations. For each PTP, two shRNA constructs were applied in this assay.

We collected cell lysates and performed immunoblotting analyses to compare the tyrosine phosphorylation change of β-catenin in the absence and presence of PTP shRNA. Under normal fetal bovine serum (FBS)-containing medium, 8 of 37 classic PTPs showed enhanced tyrosine phosphorylation of β-catenin upon shRNA knockdown: PTPN2, PTPN22, PTPN23, PTPRH, PTPRK, PTPS31, PTPRR, and PTPRU. We further stimulated cells with EGF to evaluate the function of PTP knockdown on β-catenin phosphorylation, when β-catenin SRC kinases were activated (Fig. 2*A*). Compared with luciferase shRNA control, shRNA against both PTPN23, whose function in dephosphorylating Tyr-142 of β-catenin has been recently reported by us (31), and PTPRR demonstrated elevated tyrosine phosphorylation of β-catenin on 142 (Fig. 2*B*). qRT-PCR analysis was also performed to confirm the effectiveness of shRNA knockdown in targeting all of these candidate tyrosine phosphatases (Fig. 2*C*). These results strongly suggested that PTPRR might be the tyrosine phosphatase controlling the phosphorylation level of β-catenin at Tyr-142.

PTPRR was down-regulated in ovarian carcinoma–derived cell lines, and ectopic re-expression of PTPRR led to significantly delayed cell growth in vitro and tumorigenesis in vivo

Next, we used immunoblotting to compare the expression of PTP proteins between two HOSE cell lines and 11 ovarian carcinoma-derived cell lines. In total, 13 PTP proteins were probed, including all positive hits from previous studies. The expression patterns of these 13 PTPs were divided into three categories: diminished expression, which contained PTPRR, PTPRM, and PTPRK; elevated expression, which contained PTPN2, PTPN6, PTPN11, PTPN22, PTPRS, and PTPRH; and unchanged expression, including PTPRU, PTPRJ, PTPRF, and PTPN23. We observed that the level of PTPRR was significantly down-regulated, relative to the HOSE control cells, in all ovarian carcinoma-derived cell lines (Fig. 3*A*).

To further assess the biological consequences of PTPRR loss in ovarian carcinoma–derived cells, we established stable lines (OVCAR5 w/PTPRR and CAOV4 w/PTPRR) in which PTPRR protein was ectopically expressed (Fig. 3, *B* and *D*). Ectopic expression of PTPRR-WT, but not DA mutant (substrate-trapping mutant of the phosphatase, lacking phosphatase activity), decreased the phosphorylation level of ERK1/2, a known substrate of the phosphatase (Fig. 3, *B* and *D*) (32). Concomitantly, tyrosine phosphorylation of β-catenin, but not its activating kinase SRC, was also decreased in the presence of ectopically expressed tyrosine phosphatase PTPRR (Fig. 3, *B* and *D*). Consistently, expression of WT PTPRR significantly decreased the TOP luciferase intensity, implying the inactivation of Wnt signaling (Fig. 3, *C* and *E*). We did notice a relatively mild but statistically significant difference between the parental and PTPRR-WT cell lines (Fig. 3*C*). We reasoned this to the potential functional redundancy of protein tyrosine phosphatases. As showed in Fig. 2*B*, our shRNA screen identified that knockdown of PTPRR, PTPN23, or PTPN22 could increase the phosphorylation level of β-catenin. Furthermore, restoration of PTPRR expression in ovarian tumor cells delayed cell proliferation (Fig. 3, *F* and *G*). These effects were not observed in cells with enzymatically dead trapping mutant of the phosphatase (DA mutant) (Fig. 3, *F* and *G*) or cells with SHP1 expression (Fig. 3, *H* and *I*), indicating that phosphatase activity of PTPRR was required in cell proliferation regulation.

Our observation that ovarian cancer cells with ectopically expressed PTPRR showed a reduced rate of proliferation prompted us to further investigate its role *in vivo*. We adopted a xenograft mouse model with subcutaneous injection of either parental or PTPRR-overexpressed OVCAR5 cells to evaluate whether restoration of PTPRR affected the growth of ovarian cancer cells. All cells were engineered with a luciferase cassette so that we could easily monitor tumor growth *in vivo*. Results showed that ectopic expression of PTPRR-WT, but not DA mutant, significantly delayed xenograft tumor growth (Fig. 4 (*A–C*) and Fig. S1*A*). Compared with parental OVCAR5 cells and PTPRR-DA–overexpressed tumors, tumors with PTPRR-WT overexpression showed less positive staining of Ki-67 (Fig. 4, *D* and *E*), a standard marker for cell proliferation. Using immunohistochemistry staining, we also observed decreased tyrosine phosphorylation of β-catenin on 142 in tumors with PTPRR-WT overexpression (Fig. 4, *D* and *E*).

We also used an intraperitoneal injection mouse model to further evaluate the regulatory function of PTPRR in ovarian tumor growth *in vivo*. Consistent with a previous subcutaneous injection mouse model, OVCAR5 cells with PTPRR-WT overexpression significantly decreased the number of tumor formations in the small intestine (Fig. 4*F* and Fig. S1*B*). Mice injected with PTPRR-WT–expressed tumor cells also showed less body weight loss (Fig. 4*G*). In summary, the restoration of functional PTPRR delays ovarian cancer cell proliferation both *in vitro* and *in vivo*.

PTPRR-dephosphorylated β-catenin at Tyr-142 was α-catenin–dependent

SRC, FER, and other tyrosine kinases are key regulators of Tyr-142 phosphorylation of β-catenin. We therefore investigated whether these kinases that induced phosphorylation of β-catenin at Tyr-142 were also dephosphorylated by PTPRR.

Figure 1. Aberrant activation of the Wnt/β-catenin pathway in ovarian tumors and ovarian tumor–derived cell lines. *A*, ovarian cancer with adjacent normal ovary tissue array was immunostained with antibodies against Tyr-142–phosphorylated and total β-catenin. Representative images are shown. *B*, summary and statistical analysis of immunohistochemistry staining status of ovary cancer tissue array with antibodies against Tyr-142–phosphorylated and total β-catenin. *C*, ratio analysis of pTyr-142 β-catenin–positive ovary tumor samples at different grades of the disease. *D*, ratio analysis of pTyr-142 β-catenin–positive ovary tumor samples at different stages of the disease. *E*, immunoblot analysis of pTyr-142 β-catenin with adjacent normal tissue and ovary tumor tissue. *F*, cytosolic and nuclear distribution of β-catenin in both control and ovarian carcinoma–derived cell lines. The blots were reprobed for lamin B and tubulin as nuclear and cytosolic markers, respectively. *G*, total cell lysates from both control and ovarian carcinoma–derived cell lines were immunoblotted for pTyr-142 and total β-catenin, as well as Wnt/β-catenin pathway activation markers LEF1, TCF1, TCF3, TCF4, and SFRP1, using GAPDH as a loading control. *H*, TOP/FOP reporter assay with control and ovarian carcinoma–derived cell lines. Results represent mean ± S.D. (*error bars*).

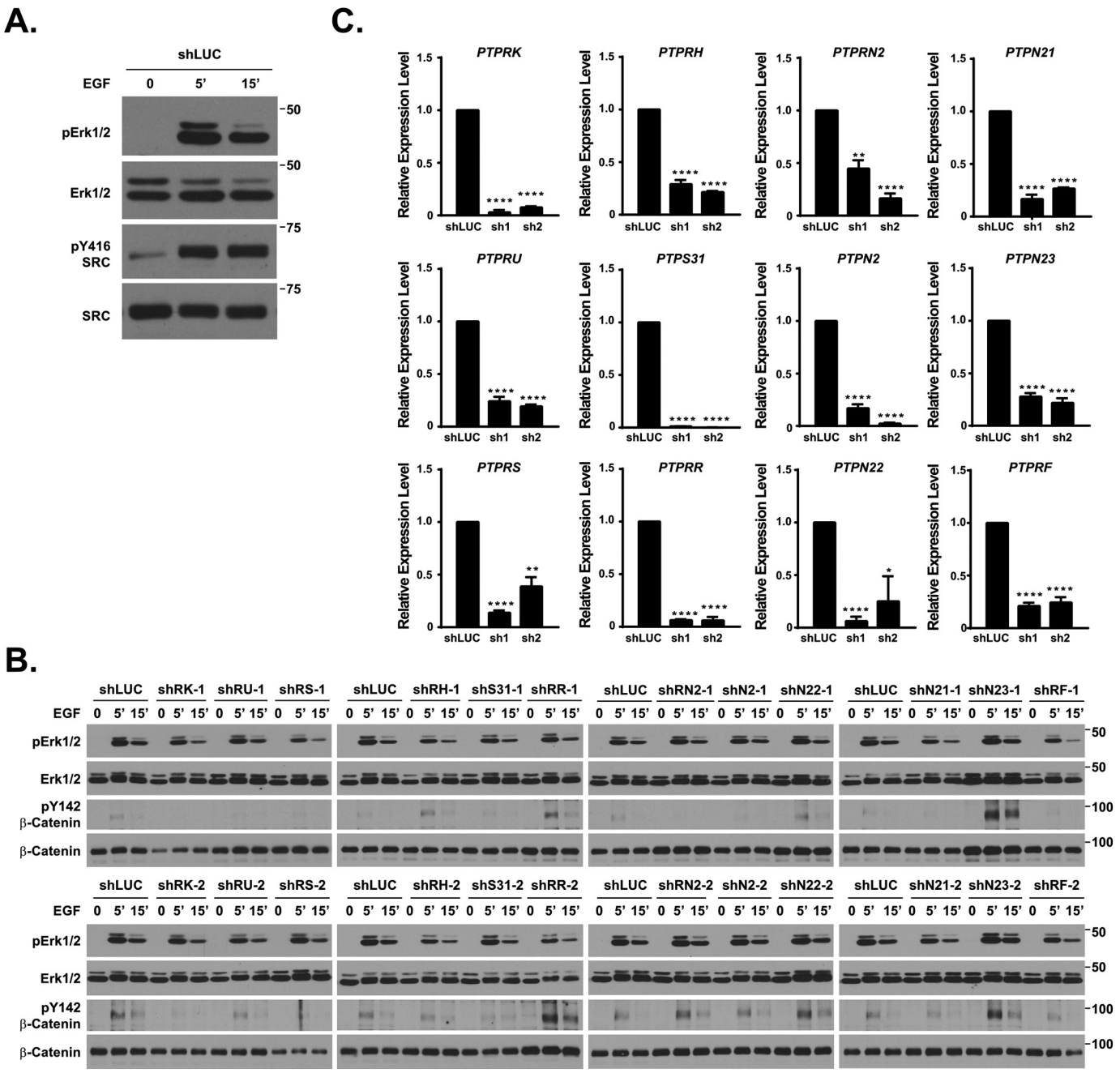

Figure 2. Protein tyrosine phosphatase screen identified PTPRR as one of the major tyrosine phosphatases responsible for dephosphorylation of β-catenin at Tyr-142. *A*, MCF10A mammary epithelial cells with luciferase control or PTP shRNAs were stimulated with EGF for the indicated times. The efficacy of the stimulation was determined by probing the activation of ERK1/2. Phosphorylation of β-catenin at Tyr-142 was also evaluated. *B*, immunoblot analysis of pTyr-416 SRC and phospho-ERK with MCF10A cells stimulated with EGF. *C*, qRT-PCR showed the knockdown efficiency of the indicated shRNAs. Data are shown as mean ± S.D. (*error bars*). *, $p < 0.05$; **, $p < 0.01$; ****, $p < 0.0001$.

Both substrate-trapping mutant (DA) and enzymatically dead mutant (CS) were also included in this study, as indicated. The results demonstrated that WT PTPRR, but not DA mutant, could dephosphorylate β-catenin on Tyr-142 in 293T cells (Fig. 5*A*). Then we investigated whether PTPRR dephosphorylates β-catenin by direct binding. The co-immunoprecipitation experiment showed that none of the WT, DA mutant, and CS mutant of PTPRR could form a complex with β-catenin (Fig. 5*B*).

We then concluded that PTPRR dephosphorylation of β-catenin was via indirect binding. It has been reported that E-cadherin, β-catenin, and α-catenin could form a complex at the plasma membrane (19–23). We then used a proximity-based tagging system, PUP-IT (pupylation-based interaction tagging) (33), to identify potential protein–protein interactions between PTPRR and E-cadherin or α-catenin as well as other proteins. A small protein tag, Pup (E), is covalently transferred to proteins that interact with a PafA-fused bait (here PTPRR), enabling transient and weak interactions to be enriched and detected by MS. We first successfully engineered an inducible ovarian cancer cell line expressing Pup (E) upon doxycycline addition. The dephosphorylation function of PafA-fused

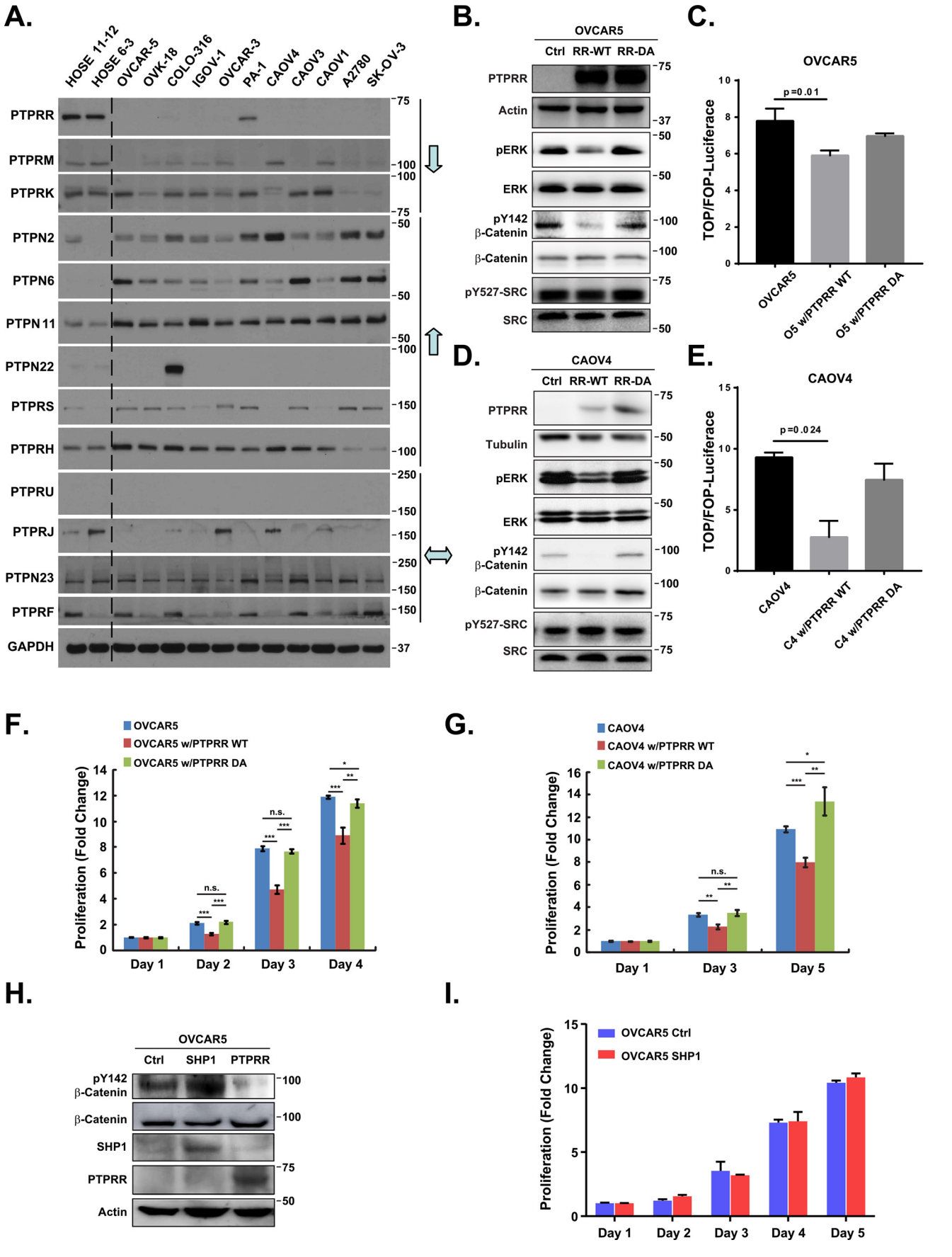
A.
HOSE 11-12
HOSE 6-3
OVCAR-5
OVK-18
COLO-316
IGOV-1
OVCAR-3
PA-1
CAOV4
CAOV3
CAOV1
A2780
SK-OV-3
PTPRR
PTPRM
PTPRK
PTPN2
PTPN6
PTPN11
PTPN22
PTPRS
PTPRH
PTPRU
PTPRJ
PTPN23
PTPRF
GAPDH
B.
OVCAR5
Ctrl RR-WT RR-DA
PTPRR
Actin
pERK
ERK
pY142 β-Catenin
β-Catenin
pY527-SRC
SRC
C.
OVCAR5
p=0.01
TOP/FOP-Luciferace
OVCAR5
O5 w/PTPRR WT
O5 w/PTPRR DA
D.
CAOV4
Ctrl RR-WT RR-DA
PTPRR
Tubulin
pERK
ERK
pY142 β-Catenin
β-Catenin
pY527-SRC
SRC
E.
CAOV4
p=0.024
TOP/FOP-Luciferace
CAOV4
C4 w/PTPRR WT
C4 w/PTPRR DA
F.
OVCAR5
OVCAR5 w/PTPRR WT
OVCAR5 w/PTPRR DA
Proliferation (Fold Change)
Day 1
Day 2
Day 3
Day 4
G.
CAOV4
CAOV4 w/PTPRR WT
CAOV4 w/PTPRR DA
Proliferation (Fold Change)
Day 1
Day 3
Day 5
H.
OVCAR5
Ctrl SHP1 PTPRR
pY142 β-Catenin
β-Catenin
SHP1
PTPRR
Actin
I.
OVCAR5 Ctrl
OVCAR5 SHP1
Proliferation (Fold Change)
Day 1
Day 2
Day 3
Day 4
Day 5

PTPRR was also confirmed by Western blotting (Fig. S2*A*). In total, 41 single-cell clones were established, and clone 9 (Fig. S2*B*) was chosen for further investigation due to its high efficiency of doxycycline induction. Then we stably expressed PTPRR (WT)-PafA or PTPRR (DA)-PafA in these inducible cells and identified Pup (E)–labeled proteins as the potential substrates for the phosphatase. The results have been deposited to the ProteomeXchange Consortium (PXD015352). Consistent with the co-immunoprecipitation experiment, we did not observe any interaction between β-catenin and either WT or DA mutant of PTPRR. We did observe strong binding between PTPRR and MAPK1, the known substrates of the phosphatase; however, the trapping mutant of the phosphatase did not show preferential binding to this substrate. We also found that α-catenin (CTNNA1) had similar strong binding to both WT and DA mutant of PTPRR (Table S2).

We performed a biochemical pulldown assay in OVCAR5 cells to further confirm the results from the PTPRR PUP-IT experiment. Using a reciprocal immunoprecipitation assay, we found that PTPRR formed a complex with α-catenin (Fig. 5, *C* and *D*). In line with previous reports, α-catenin also formed a complex with E-cadherin and β-catenin in OVCAR5 cells (Fig. 5, *E* and *F*). These results implied that α-catenin may mediate the recruitment of PTPRR near β-catenin for subsequent dephosphorylation.

We then used shRNA to knock down α-catenin in both parental and PTPRR-WT–expressed OVCAR5 cells to examine whether the recruitment of PTPRR by α-catenin was required for β-catenin dephosphorylation on site 142 (Fig. 5, *G* and *H*). First, PTPRR expression significantly reduced the phosphorylation level of Tyr-142 β-catenin (Fig. 5*H*, *lane 1 versus lane 4*). Second, in parental OVCAR5 cells with no PTPRR expression, loss of α-catenin had minimal effect on tyrosine phosphorylation of β-catenin (Fig. 5*H*, *lane 1 versus lanes 2* and *3*). On the contrary, in OVCAR5 cells with ectopic PTPRR-WT expression, tyrosine phosphorylation of β-catenin on Tyr-142 was increased upon α-catenin knockdown (Fig. 5*H*, *lane 4 versus lanes 5* and *6*). Third, cell fractionation analysis demonstrated nuclear accumulation of pTyr-142, and total β-catenin was reduced by PTPRR in an α-catenin–dependent manner (Fig. S3). Taken together, our data demonstrated that α-catenin could form a complex with E-cadherin, β-catenin, and PTPRR, and its association with PTPRR is required for dephosphorylation and nuclear accumulation of β-catenin by the phosphatase.

ARID3C was identified as one of the major β-catenin downstream targets in controlling ovarian cancer cell proliferation

Next, we conducted RNA-Seq to further evaluate the impact of PTPRR-mediated β-catenin dephosphorylation on changes in transcription profiling in both ovarian cancer cells and xenograft tumors. Results from OVCAR5 cells with or without ectopic expression of either PTPRR-WT or DA mutant are illustrated in Fig. 6*A* (and GEO database entry GSE135220), with -fold change $\leq 2^{\wedge}(-0.5)$ or $\geq 2^{\wedge}(0.5)$ highlighted. Genes meeting the following criteria were defined as responsive genes: (i) -fold change $\leq 2^{\wedge}(-0.5)$ or $\geq 2^{\wedge}(0.5)$ in both parental OVCAR5 and PTPRR-DA–overexpressed OVCAR5 cells; (ii) $2^{\wedge}(-0.5) \leq$ -fold change $\leq 2^{\wedge}(0.5)$ in PTPRR-WT–overexpressed OVCAR5 cells. The experiment was repeated twice. In total, 1,267 genes were identified (Fig. 6*E*), and KEGG database analysis of these genes suggested that the Wnt signaling pathway was significantly enriched (Fig. 6*B*).

We did the same RNA-Seq analysis in xenograft tumor samples (Fig. 6*C* and GEO database entry GSE135220). In total, 1,817 candidate genes that were significantly changed in tumors with PTPRR-WT expression were identified (Fig. 6*E*). To pinpoint PTPRR responsive genes, we analyzed RNA-Seq data from both cell lines and xenograft tumor samples and defined candidates as the overlapped significantly changed genes. In total, 97 PTPRR responsive genes were identified and illustrated in Fig. 6*D*. All of these genes were further filtered by a previously published ChIP-Chip data set of β-catenin (34). Through all of these analyses, ARID3C, PBXIP1, and DVL3 were demonstrated as β-catenin–targeted genes, and their expression levels were regulated by PTPRR in ovarian cancer cells (Fig. 6*E*).

We performed qRT-PCR to confirm the expression patterns of these three genes in OVCAR5 cells with or without ectopic expression of either PTPRR-WT or DA mutant, as well as in xenograft tumor samples with injection of either parental, PTPRR-WT, or PTPRR-DA–expressed OVCAR5 cells (Fig. 6, *F–H*). Expression patterns of the three genes met the criteria of "responsive gene" (the expression level must be significantly down-regulated in cells with PTPRR-WT overexpression while showing no significant difference in cells with PTPRR-DA overexpression), with ARID3C (AT-rich interactive domain-containing protein 3C) as the best fit (Fig. 6*F*). Furthermore, we did ChIP-PCR analysis to further pinpoint the binding region of β-catenin on the promoter of ARID3C (Fig. 6*I*). The result was

Figure 3. PTPRR was significantly down-regulated in ovarian carcinoma–derived cell lines and functioned as a tumor suppressor *in vitro*. *A*, two immortalized human normal ovarian epithelial cell lines (HOSE11-12 and HOSE6-3) and 11 ovarian carcinoma-derived cell lines were examined by immunoblotting to demonstrate decreased expression of PTPRR in all of the ovarian carcinoma–derived cell lines compared with normal controls. Twelve additional protein tyrosine phosphatases were also determined. GAPDH was probed as the loading control. *B* and *D*, retroviral constructs pWZL-PTPRR-WT and PWZL-PTPRR-DA were used to generate stable cell lines OVCAR5 w/PTPRR (WT or DA) and CAOV4 w/PTPRR (WT or DA). Immunoblotting was performed to demonstrate ectopic expression of PTPRR, both WT and inactive DA mutant, in ovarian carcinoma-derived cell lines OVCAR5 (*B*) and CAOV4 (*D*). Phosphorylation of ERK1/2, β-catenin at Tyr-142, and SRC at Tyr-527 were also determined. *C* and *E*, TOP/FOP reporter assay with OVCAR5 (*C*) and CAOV4 (*E*) with either Luc control, PTPRR-WT, or PTPRR-DA expression. Results represent mean ± S.D. (*error bars*). Experiments were repeated three times. Statistic analysis were calculated using a *t* test. *F* and *G*, ectopic expression of PTPRR decreased proliferation of ovarian carcinoma–derived cell lines OVCAR5 (*F*) and CAOV4 (*G*). Proliferation was assessed by a Cell Titer-Glo luminescent cell viability assay at the indicated time intervals. Results represent mean ± S.D. from three independent experiments. *H*, immunoblot analysis to demonstrate ectopic expression of PTPRR, SHP1, and control vector (pCDNA3.1 vector) in ovarian carcinoma–derived cell lines OVCAR5. Phosphorylation of β-catenin at Tyr-142 was determined. *I*, proliferation was assessed by the Cell Titer-Glo luminescent cell viability assay at the indicated time intervals with cells with either control or SHP1 expression. Results represent mean ± S.D. from three independent experiments. *n.s.*, not significant.

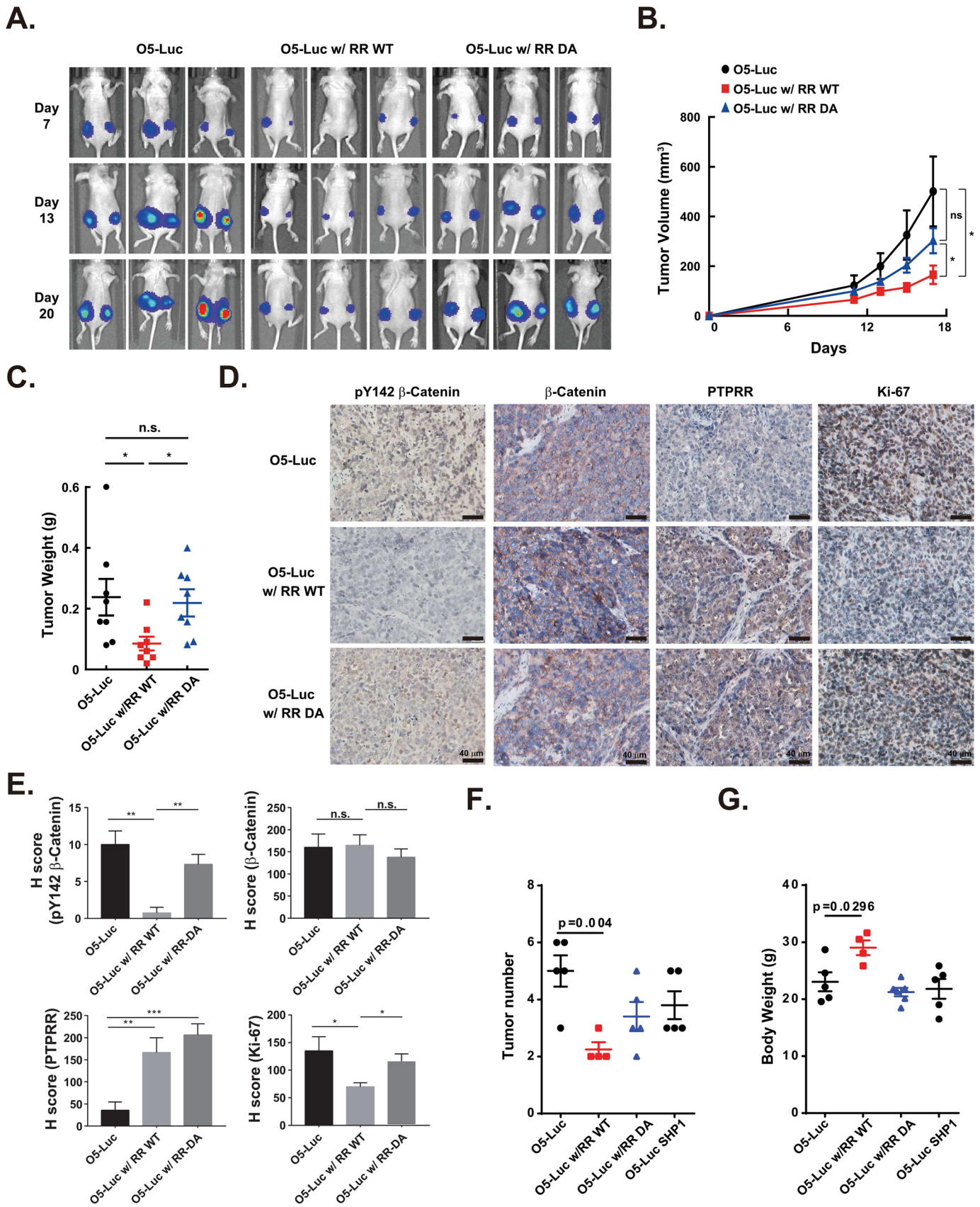
A.
O5-Luc
O5-Luc w/ RR WT
O5-Luc w/ RR DA
Day 7
Day 13
Day 20
B.
O5-Luc
O5-Luc w/ RR WT
O5-Luc w/ RR DA
Tumor Volume (mm³)
Days
ns
*
*
C.
n.s.
Tumor Weight (g)
O5-Luc
O5-Luc w/RR WT
O5-Luc w/RR DA
D.
pY142 β-Catenin
β-Catenin
PTPRR
Ki-67
O5-Luc
O5-Luc w/ RR WT
O5-Luc w/ RR DA
40 μm
E.
H score (pY142 β-Catenin)
H score (β-Catenin)
H score (PTPRR)
H score (Ki-67)
n.s.
O5-Luc
O5-Luc w/ RR WT
O5-Luc w/ RR-DA
F.
Tumor number
p =0.004
O5-Luc
O5-Luc w/RR WT
O5-Luc w/RR DA
O5-Luc SHP1
G.
Body Weight (g)
p =0.0296
O5-Luc
O5-Luc w/RR WT
O5-Luc w/RR DA
O5-Luc SHP1

consistent with the previous report (34), indicating that the transcriptional regulation of ARID3C was under the control of β-catenin.

To further evaluate the function of ARID3C in ovarian cancer cell proliferation, we performed shRNA knockdown of ARID3C in both OVCAR5 cell lines with or without ectopic PTPRR-WT (Fig. 6*J*), followed by a Cell Titer-Glo (CTG) assay. We found that ARID3C knockdown could robustly inhibit cell proliferation only in parental OVCAR5 cells and not in cells with ectopic PTPRR-WT expression (Fig. 6*K*), revealing ARID3C as one of the major downstream target genes of the PTPRR-β-catenin signaling axis in controlling ovarian cancer cell proliferation.

PTPRR was underexpressed in ovarian cancers, and its down-regulation was inversely correlated with prognosis

In support of these functional studies of PTPRR in ovarian cancer cells, we searched the Human Protein Atlas to compare the protein expression level of the phosphatase between normal ovary and malignant ovarian carcinomas. In line with our findings, we observed lower expression of PTPRR in ovarian cancer patient samples (Fig. 7*A*); in contrast, the phosphatase was highly expressed in normal ovary tissue (Fig. 7*A*).

We collected normal fallopian tube and ovary samples ($n = 12$) as well as ovarian tumor samples ($n = 18$) to further explore the expression differences of PTPRR and its impact on Tyr-142 phosphorylation of β-catenin by immunohistochemistry (Fig. 7*B*). Consistent with the results obtained from the Human Protein Atlas database, the expression level of PTPRR was significantly decreased in ovarian cancer patient samples compared with normal control (Fig. 7*C*). Furthermore, we observed a higher extent of phosphorylation on β-catenin within the patient cohort (Fig. 7*D*), and a significant negative correlation between PTPRR expression and phosphorylation intensity of Tyr-142 β-catenin was present among 18 tumor samples (Fig. 7*E*).

Finally, we analyzed clinical data from over 1,000 ovarian cancer patients (http://kmplot.com/analysis/)[5] (58) to further investigate the relationship between PTPRR expression and tumor progression. The data indicated that expression of PTPRR was a good prognostic indicator for overall survival parameters of the patient (Fig. 7*F*). The extent of separation was even significant within patient cohorts suffering from grade 1 and grade 2 disease (Fig. 7*G*).

Discussion

The core Wnt/β-catenin signaling pathway signal transduction cascade is one of the main regulators of development throughout the animal kingdom (35). Mutated Wnt pathway components are causative in multiple types of cancers (36–38). However, the frequencies of mutations in the Wnt/β-catenin pathway are relatively low in serous, clear cell, and mucinous ovarian carcinomas (11). But the components of the pathway and β-catenin targeted genes are still important in ovarian cancer development (10). Phosphorylation of two tyrosine residues in β-catenin, tyrosine 142 and 654, activates the Wnt/β-catenin pathway (20). Tyrosine kinases, including SRC, Fyn, and FER, are responsible for phosphorylation of these sites (19–23). Whereas several PTPs have been suggested as β-catenin phosphatases (30), the identity of the phosphatase that is responsible for dephosphorylation of β-catenin at Tyr-142 is still missing, especially within the ovarian cancer context.

In this study, we revealed aberrant activation of the Wnt/β-catenin pathway in ovarian patient samples and ovarian tumor-derived cell lines. Through selection with shRNA against all 37 classic protein tyrosine phosphatases, we identified PTPRR as one of the major tyrosine phosphatases responsible for dephosphorylation of β-catenin at Tyr-142. We found that PTPN23 knockdown also up-regulated the phosphorylation of Tyr-142 β-catenin (Fig. 2*B*), but the expression of PTPN23 was not down-regulated in ovarian cancer cell lines (Fig. 3*A*). Thus, we focused on PTPRR in our studies. The PTPRR gene maps to chromosome 12, and the protein encoded by this gene is a member of the protein tyrosine phosphatase (PTP) family. By methylomic approaches, PTPRR was discovered to be methylation-silenced in invasive cervical cancer (39). In acute myeloid leukemia patients, somatic mutations of PTPRR are identified using a whole-genome sequencing approach (40). Expression of PTPRR was reported to be low in oral squamous cell carcinoma (41), prostate cancer cells (42), and pancreatic cancer patient samples (43). In addition, ectopic expression of PTPRR by site-specific lentiviral injections in a mouse model resulted in increased ERK dephosphorylation, which revealed that ERK might be one of the substrates of PTPRR (44). Our study showed that decreased PTPRR expression–induced hyperactivation of β-catenin was required for ovarian cancer oncogenesis. All of these studies and ours reinforce the importance of PTPRR in tumor progression and its tumor suppressor functions. It is thus essential to identify the physiological substrates of PTPRR and the relevant signaling pathways it regulates.

We next combined PTP substrate trapping strategy with the PUP-IT system to identify the potential binding partner of PTPRR. Consistent with the co-immunoprecipitation experiment, we did not observe any interaction between β-catenin and PTPRR. However, α-catenin showed similar strong binding to either WT or DA mutant of PTPRR. By knocking down α-catenin, we found that the dephosphorylation of Tyr-142 β-catenin by PTPRR was suppressed (Fig. 5*H*), indicating the

[5] Please note that the JBC is not responsible for the long-term archiving and maintenance of this site or any other third party hosted site.

Figure 4. Ectopic re-expression of PTPRR led to significantly delayed tumorigenesis *in vivo*. *A*, at the indicated time points, mice injected with OVCAR5 cells expressing either luciferase control ($n = 6$), WT PTPRR ($n = 6$), or DA mutant PTPRR ($n = 6$) were imaged using IVIS-200 bioluminescence imaging. Representative images are shown. *B* and *C*, measurements of subcutaneous tumor volume (*B*) and weight (*C*) for mice injected with either Luc control, PTPRR-WT, or PTPRR-DA cells. Results represent mean ± S.D. (*error bars*). $n = 6$. *D*, immunohistochemistry staining (pTyr-142 and total β-catenin, PTPRR, and Ki-67) of subcutaneous tumor sections from mice injected with OVCAR5 cells expressing either luciferase control, WT PTPRR, or DA mutant PTPRR. *E*, statistical analysis of immunohistochemistry staining (pTyr-142 and total β-catenin, PTPRR, and Ki-67). Results represent mean ± S.D. *, $p < 0.05$; **, $p < 0.01$; ***, $p < 0.001$; *n.s.*, not significant. *F* and *G*, measurements of tumor number (*F*) and body weight (*G*) for mice intraperitoneally injected with either Luc control, PTPRR-WT, PTPRR-DA, or SHP1 cells. Results represent mean ± S.D. $n = 5$.

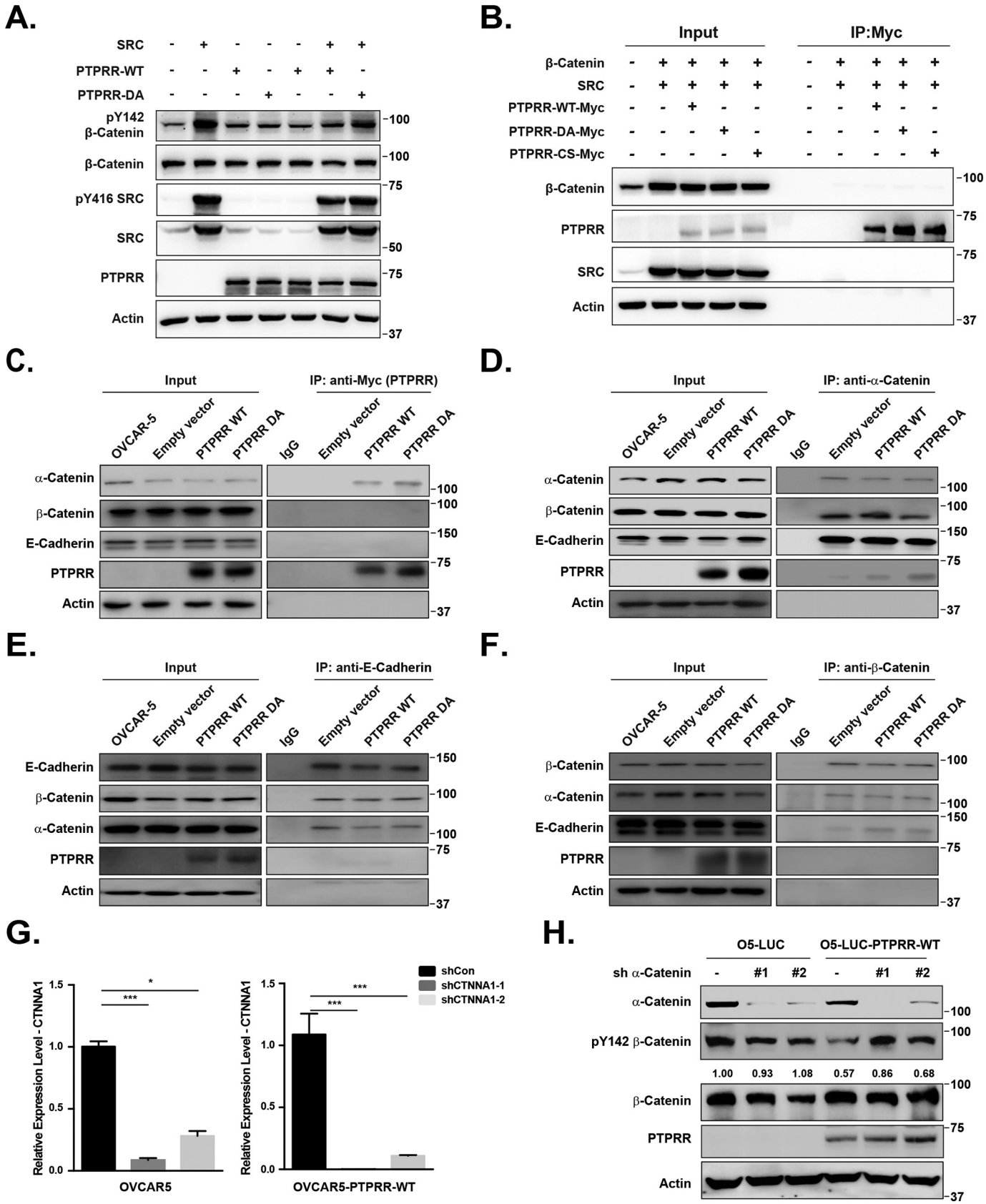
A.
SRC
PTPRR-WT
PTPRR-DA
pY142 β-Catenin
β-Catenin
pY416 SRC
SRC
PTPRR
Actin
B.
Input
IP:Myc
β-Catenin
SRC
PTPRR-WT-Myc
PTPRR-DA-Myc
PTPRR-CS-Myc
PTPRR
Actin
C.
Input
IP: anti-Myc (PTPRR)
OVCAR-5
Empty vector
PTPRR WT
PTPRR DA
IgG
α-Catenin
β-Catenin
E-Cadherin
PTPRR
Actin
D.
Input
IP: anti-α-Catenin
E.
Input
IP: anti-E-Cadherin
F.
Input
IP: anti-β-Catenin
G.
Relative Expression Level - CTNNA1
shCon
shCTNNA1-1
shCTNNA1-2
OVCAR5
OVCAR5-PTPRR-WT
H.
O5-LUC
O5-LUC-PTPRR-WT
sh α-Catenin
α-Catenin
pY142 β-Catenin
1.00 0.93 1.08 0.57 0.86 0.68
β-Catenin
PTPRR
Actin

necessity of α-catenin during this dephosphorylation. We also confirmed that β-catenin formed a complex with α-catenin and E-cadherin in ovarian cancer cell lines by immunoprecipitation. Thus, we concluded that PTPRR dephosphorylation of β-catenin is α-catenin–dependent.

With RNA-Seq and ChIP-PCR analysis, we found that ARID3C is a novel downstream target of the PTPRR-β-catenin cascade in ovarian cancer cells. ARID3C was recently characterized as one of the AT-rich interactive domain (ARID) family proteins featuring a highly conserved, helix-turn-helix DNA-binding domain (45, 46). Proteins with this domain bind to the major groove of DNA and are involved in functions ranging from chromatin remodeling to cell cycle control (45, 47). Although studies on ARID3C are still limited, its two closely related paralogues, ARID3A and ARID3B, are reported to be associated with tumorigenesis (48–50). In particular, ARID3B is elevated in serous ovarian cancer patients (51, 52), and overexpression of ARID3B in ovarian cancer cells accelerates tumor growth *in vitro* and *in vivo* (53). Therefore, it will be interesting to further characterize the function of ARID3C, a novel downstream target of the Wnt/β-catenin pathway, in PTPRR-deficient ovarian cancer cells.

Overall, through a shRNA screen among all classic tyrosine phosphatases, we identified the protein-tyrosine phosphatase PTPRR responsible for tyrosine dephosphorylation of β-catenin on Tyr-142, a key site controlling transcriptional activity of β-catenin. Remarkably, PTPRR was down-regulated in ovarian cancers, and ectopic re-expression of the phosphatase led to significantly delayed ovarian cancer cell growth *in vitro* and *in vivo*. The results of this study suggest that the expression level of the phosphatase could be a good prognostic marker for overall survival of patients.

Experimental procedures

Tissue array analysis

A commercial ovarian tissue array was used for this analysis (OV2001a, Biomax US). This tissue array includes both eight adjacent normal ovary tissues, which are widely used as normal control, and ovarian tumors, including 133 cases of serous carcinoma, 34 mucinous adenocarcinoma, 3 adenocarcinoma, 7 endometrioid adenocarcinoma, and 15 metastatic carcinoma. This tissue array also includes information about TNM and FIGO classification and staging of tumors of the ovary, fallopian tube, and primary peritoneal carcinoma. Antibodies used in this staining were pTyr-142 and total β-catenin (CP1081 and CM1181, ECM Bioscience).

PTP shRNA library construction and infection

The details for PTP shRNA library construction, including shRNA sequences, were described by Lin *et al.* (54). In brief, a retroviral expression vector, pMLP (MSCV-based vector expressing shRNA in a miR30 context), was used to construct this shRNA library. This vector contains puromycin resistance marker and an EGFP marker for stable cell line selection. The RNAi Codex program (59) was applied to generate shRNA sequence for each protein tyrosine phosphatase. shRNA retrovirus was generated in Phoenix-Ampho packaging cells by co-transfecting plasmids, including pMLP, VSVG, and the pCL-Ampho retrovirus packaging vector, at a ratio of 3:1:1. 24 h after transfection, recombinant retrovirus supernatants were harvested. The cleared supernatants were then incubated with MCF10A cells in the presence of Polybrene (8 mg/ml final concentration). 24 h after infection, cells were placed under puromycin selection (2 mg/ml final concentration) for generating a PTP knockdown stable cell line.

MCF10A cells were lysed in radioimmune precipitation buffer (50 mM Tris-Cl, pH 7.4, 150 mM NaCl, 1% Nonidet P-40, 1% sodium deoxycholate, 0.1% SDS, 50 mM NaF, 1 mM Na_3VO_4, 10% glycerol, protease inhibitor mixture from Roche Applied Science) at 4 °C for 30 min.

Cell culture

Ovarian carcinoma–derived cell lines were cultured in Dulbecco's modified Eagle's medium supplemented with 10% FBS, penicillin (100 units/ml), and streptomycin (100 μg/ml). Normal HOSE11-12 and HOSE6-3 control cell lines were grown in 199/MCDB 105 (1:1) medium containing 10% FBS. Cells were maintained at 37 °C in an atmosphere of 5% CO_2.

Cell transfection

PTPRR cDNA (NM_002849 658aa) was used in this study. The DA mutant of PTPRR was a point mutation at D554A based on PTPRR-WT cDNA. The CS mutant of PTPRR was a point mutation at C588S based on PTPRR-WT cDNA. These cDNAs were cloned into the expression plasmids pCDNA3.1 and pWZL.

Cells were transfected with plasmids by using transfection reagent Mirus (TransIT-2020, Mirus Bio), following the supplier's guidance. Briefly, cells were plated in a 6-well plate on the first day. TransIT:DNA complexes were prepared by combining Opti-MEM I reduced-serum medium, plasmid DNA, and TransIT® reagent and adding to cells on the second day. Cells were harvested for further studies 24 h after the transfection.

TOP/FOP reporter assay

We transfected cells with TOP or FOP flash plasmids along with SV40-*Renilla* plasmid (control for transfection) using transfection reagent Mirus (TransIT-2020, Mirus Bio). Two days after transfection, we detected luciferase activity using the

Figure 5. PTPRR dephosphorylated β-catenin at Tyr-142 was α-catenin–dependent. *A*, 293T cells were transiently transfected with SRC, PTPRR-WT, or DA mutant (in pCDNA3.1 vector), as indicated. Tyrosine phosphorylation of β-catenin at Tyr-142 was compared. Expression of β-catenin, PTPRR, and loading control actin were also probed. *B*, after transient transfection with β-catenin, SRC, Myc-tagged PTPRR-WT, DA, or CS mutant (in pCDNA3.1 vector), as indicated, PTPRR was immunoprecipitated with resin against Myc tag and probed for association with β-catenin and SRC. *C–F*, 293T cells were transiently transfected with Myc-tagged PTPRR-WT or DA mutant (in pCDNA3.1 vector), as indicated. PTPRR (*C*), α-catenin (*D*), E-cadherin (*E*), and β-catenin (*F*) were immunoprecipitated. The association of PTPRR, α-catenin, β-catenin, and E-cadherin was assessed. *G*, representative qRT-PCR analysis detecting CTNNA1 expression level in OVCAR5 cells with or without CTNNA1 knockdown. The experiment was done in triplicate. Data are shown as means ± S.E. (*error bars*). *H*, OVCAR5 cells and PTPRR-WT ectopically expressed OVCAR5 cells were stably transfected with CTNNA1 shRNA as indicated. Tyrosine phosphorylation of β-catenin at Tyr-142 were normalized to total expression level of β-catenin. Expression of α-catenin, PTPRR, and loading control actin were also probed.

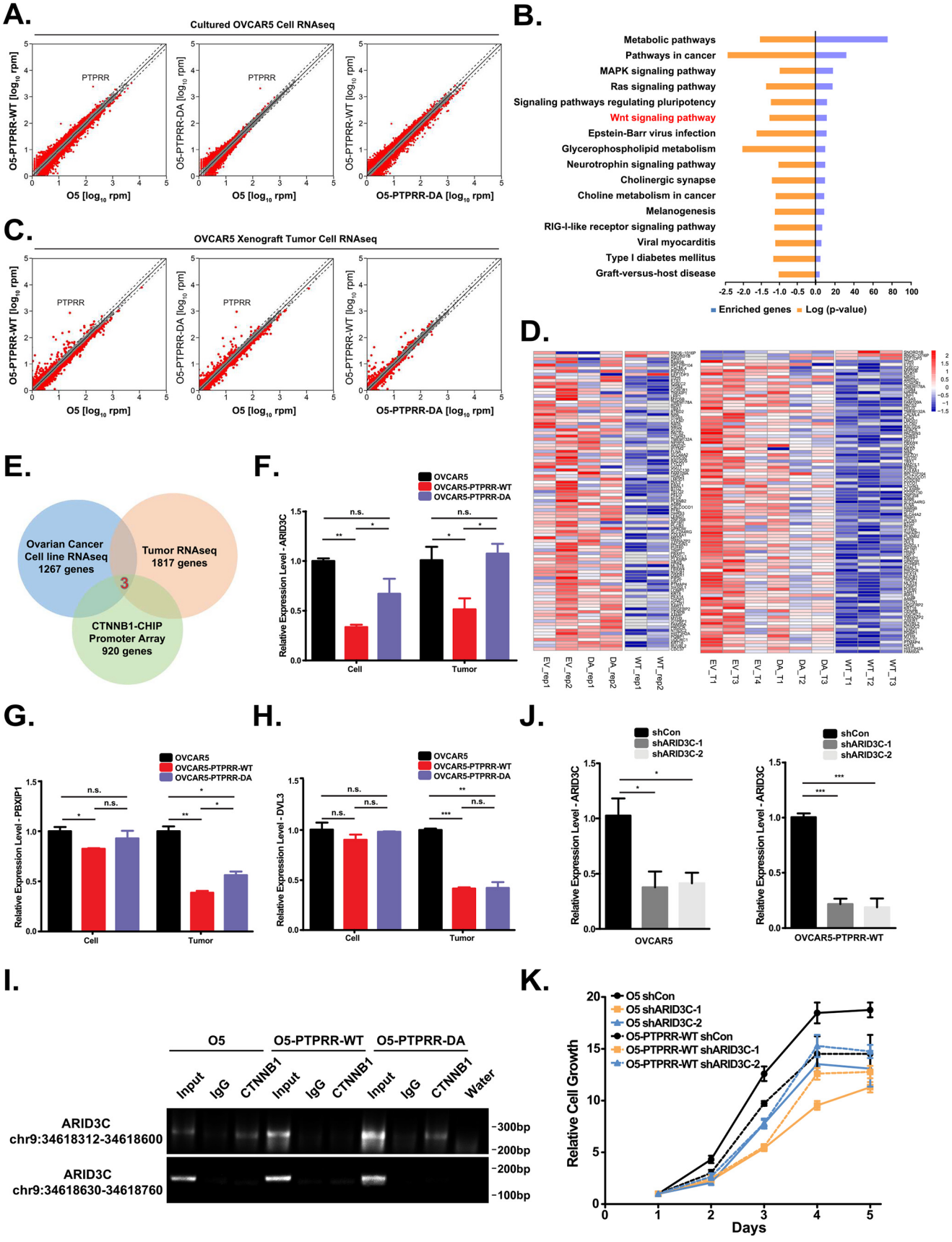
A.
Cultured OVCAR5 Cell RNAseq
PTPRR
O5-PTPRR-WT [log10 rpm]
O5 [log10 rpm]
O5-PTPRR-DA [log10 rpm]
B.
Metabolic pathways
Pathways in cancer
MAPK signaling pathway
Ras signaling pathway
Signaling pathways regulating pluripotency
Wnt signaling pathway
Epstein-Barr virus infection
Glycerophospholipid metabolism
Neurotrophin signaling pathway
Cholinergic synapse
Choline metabolism in cancer
Melanogenesis
RIG-I-like receptor signaling pathway
Viral myocarditis
Type I diabetes mellitus
Graft-versus-host disease
Enriched genes
Log (p-value)
C.
OVCAR5 Xenograft Tumor Cell RNAseq
D.
EV_rep1
EV_rep2
DA_rep1
DA_rep2
WT_rep1
WT_rep2
EV_T1
EV_T3
EV_T4
DA_T1
DA_T2
DA_T3
WT_T1
WT_T2
WT_T3
E.
Ovarian Cancer Cell line RNAseq 1267 genes
Tumor RNAseq 1817 genes
3
CTNNB1-CHIP Promoter Array 920 genes
F.
OVCAR5
OVCAR5-PTPRR-WT
OVCAR5-PTPRR-DA
Relative Expression Level - ARID3C
Cell
Tumor
G.
Relative Expression Level - PBXIP1
H.
Relative Expression Level - DVL3
J.
shCon
shARID3C-1
shARID3C-2
Relative Expression Level - ARID3C
OVCAR5
OVCAR5-PTPRR-WT
I.
O5
O5-PTPRR-WT
O5-PTPRR-DA
Input
IgG
CTNNB1
Water
ARID3C chr9:34618312-34618600
ARID3C chr9:34618630-34618760
300bp
200bp
100bp
K.
O5 shCon
O5 shARID3C-1
O5 shARID3C-2
O5-PTPRR-WT shCon
O5-PTPRR-WT shARID3C-1
O5-PTPRR-WT shARID3C-2
Relative Cell Growth
Days

Dual-Luciferase reporter assay system (FR201-01, Transgen Biotech) according to the manufacturer's protocol.

Cell proliferation assay

The Cell Titer-Glo (CTG) luminescent cell viability assay (Promega) was used to evaluate the role of PTPRR in ovarian cancer cell proliferation. In brief, 1.5×10^3 cells (OVCAR5 and CAOV4) per well were seeded in a 96-well plate and grown for the indicated time intervals. CTG reagent was added to each well and mixed for ~15 min on an orbital shaker to induce cell lysis, followed by luminescence reading. Results represent mean ± S.E. from three independent experiments.

Cell fractionation assay

We used the NE-PER nuclear and cytoplasmic extraction reagents kit (catalog no. 78833) to extract nuclear and cytosolic compartments of control and ovarian cancer cell lines, following the manufacturer's protocol. Lamin B and tubulin were used as nuclear and cytosolic markers, respectively.

PUP-IT mass spectrometry

The experimental procedure was modified based on a previous study (33). To generate iPUP (inducible Pup) cell lines, we produced lentivirus with the PUP (E) plasmid (Bio-Pup (E)-IRES-BFP within the Tet-On system) and infected OVCAR5 cells for 48 h. 2 μg/ml doxycycline (SELLECK, S4136) was added into the culture medium for another 24 h. After that, BFP-positive cells were sorted into 96-well plates for single clone selection. Two weeks later, each clone was examined for BFP expression by flow cytometry with or without doxycycline. The expression of Bio-Pup (E) in BFP-positive cells was also confirmed by Western blot analysis.

To further stably express PTPRR (WT)-PafA or PTPRR (DA)-PafA in iPUP OVCAR5 cells, we subcloned PTPRR-WT or -DA, respectively, into the PafA-IRES-EGFP plasmid. Each plasmid was packed into a lentivirus and then transduced into iPUP OVACR5 cells for 48 h. GFP-positive cells were sorted by flow cytometry. The expression of PTPRR (WT)-PafA and PTPRR (DA)-PafA was confirmed by Western blot analysis.

PTPRR (WT)-PafA or PTPRR (DA)-PafA expressed iPUP OVCAR5 cells were grown to a cell density of about 75% on 10-cm dishes. We followed the protocol established in the study by Liu *et al.* (33). We used trypsin to generate peptides. To prepare PUP-IT samples for MS analysis, we used doxycycline induction, biotin labeling, cell lysis, streptavidin magnetic beads pulldown, trypsin digestion, and peptide cleaning.

An Easy-nLC 1000 system coupled to a Q Exactive HF (both from Thermo Scientific) was used to separate and analyze peptides (33). About 1 μg of peptides were separated in an Easy-Spray C18 column (75 μm × 50 cm, 2 μm, 100 Å, Thermo Scientific) at a flow rate of 250 nl/min at 50 °C. Mobile phase A (0.1% formic acid in water) and mobile phase B (0.1% formic acid in 98% acetonitrile) were used to establish a 60-min gradient composed of 1 min of 4% B, 48 min of 4–26% B, 1 min of 26–30% B, 1 min of 30–70% B, and 9 min of 70% B. Electrospray was set to 2.35 kV for ionizing peptides. The following conditions were used to acquire a full MS spectrum (300–1400 m/z range): resolution of 120,000 at m/z 200 and a maximum ion accumulation time of 20 ms. Dynamic exclusion was 30 s. Resolution for HCD MS/MS spectra was 30,000 at m/z 200. The automatic gain control settings of MS1 and MS2 were 3E6 and 1E5, respectively. The 20 most intense ions above a 3.3E4 count threshold were selected for fragmentation by HCD with a maximum ion accumulation time of 60 ms. An isolation width of 1.6 m/z units was used for MS2. We excluded single and unassigned charged ions from MS/MS. Normalized collision energy was 25% for HCD.

The raw data were processed and searched with MaxQuant version 1.5.4.1 with MS tolerance of 4.5 ppm and MS/MS tolerance of 20 ppm. The UniProt human protein database (release 2016_07, 70,630 sequences) and a database for proteomics contaminants from MaxQuant were used for database searches. Reversed database searches were used to evaluate false discovery rate (FDR) of peptide and protein identifications. Two missed cleavage sites of trypsin were allowed. Oxidation (M), pyro-Glu (Gln at peptide N terminus), acetyl (Protein N-term), deamidation (NQ), and GGE (K) were set as variable modifications. We set the FDR of both peptide identification and protein identification to 1%. We also enabled the options of "Second peptides," "Match between runs," and "Dependent peptides." Label-free quantification was used to quantify the difference in protein abundances between different samples.

We compared the difference in terms of binding proteins between OVCAR5 cells with PTPRR-WT expression and cells with PTPRR-DA expression. To obtain reliable quantification measurement, each group sample was triplicated. To analyze

Figure 6. ARID3C was identified as one of the major β-catenin downstream targets in controlling ovarian cancer cell proliferation. *A*, comparison of steady-state RNA levels are shown as reads per million (*rpm*), from pre-injected OVCAR5 cells, PTPRR-WT expressed OVCAR5 cells, and PTPRR-DA expressed OVCAR5 cells. *Dashed lines*, 2^0.5-fold changes. All genes above this threshold are represented as *red dots*. The average of two replicates is shown. *B*, KEGG pathways commonly containing significantly changed DEGs. *C*, comparison of steady-state RNA levels are shown as reads per million, from tumor cells derived from OVCAR5 cell, PTPRR-WT– expressed OVCAR5 cell, and PTPRR-DA– expressed OVCAR5 cell injection. *Dashed lines*, 2^0.5-fold changes. All genes above this threshold are represented as *red dots*. The average of three replicates is shown. *D*, heat map of significantly changed genes in both cell line RNA-Seq and tumor tissue RNA-Seq. *E*, overlap of significantly changed genes from ovarian cancer cell line RNA-Seq and tumor tissue RNA-Seq with targeted genes from the CTNNB1-CHIP promoter array (GSE21151). *F*, representative qRT-PCR analysis detecting ARID3C expression level in cells and tumors from OVCAR5 cell, PTPRR-WT– expressed OVCAR5 cell, and PTPRR-DA– expressed OVCAR5. The experiment was done in triplicate. Data are shown as means ± S.E. (*error bars*). *G*, representative qRT-PCR analysis to detect the PBXIP1 expression level in cells and tumors from OVCAR5 cells, PTPRR-WT– expressed OVCAR5 cell, and PTPRR-DA– expressed OVCAR5. The experiment was done in triplicate. Data are shown as means ± S.E. *H*, representative qRT-PCR analysis detecting DVL3 expression level in cells and tumors from OVCAR5 cells, PTPRR-WT– expressed OVCAR5 cells, and PTPRR-DA– expressed OVCAR5. The experiment was done in triplicate. Data are shown as means ± S.E. *I*, ChIP-PCR assay confirming the binding of CTNNB1 to the promoter region of ARID3C in OVCAR5 and PTPRR-DA– expressed OVCAR5 cells but not PTPRR-WT– expressed OVCAR5 cells. *J*, representative qRT-PCR analysis detecting ARID3C expression level in OVCAR5 cells and PTPRR-WT– expressed OVCAR5 cells with or without ARID3C shRNA knockdown. The experiment was done in triplicate. Data are shown as means ± S.E. *K*, cell proliferation assay on OVCAR5 and PTPRR-WT– expressed OVCAR5 cells with and without ARID3C knockdown. The experiment was done in hexatriplicate. Data are shown as means ± S.E. *n.s.*, not significant.

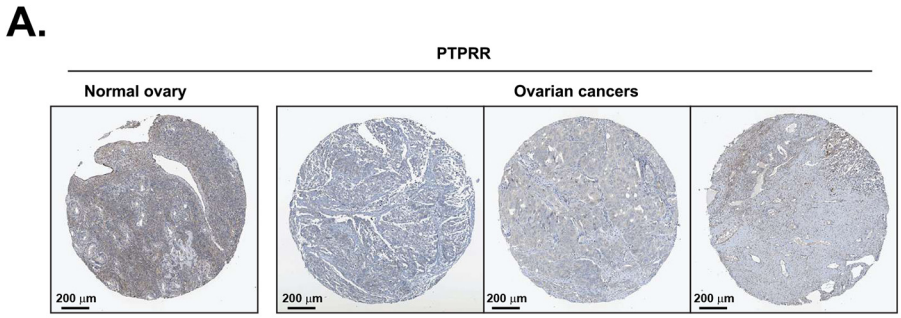

Gene	Antibody	Ptotein Level				
		Normal ovary	Ovarian cancers			
			ND	Low	Medium	High
PTPRR	CAB011461	Medium	1/12	7/12	4/12	0/12

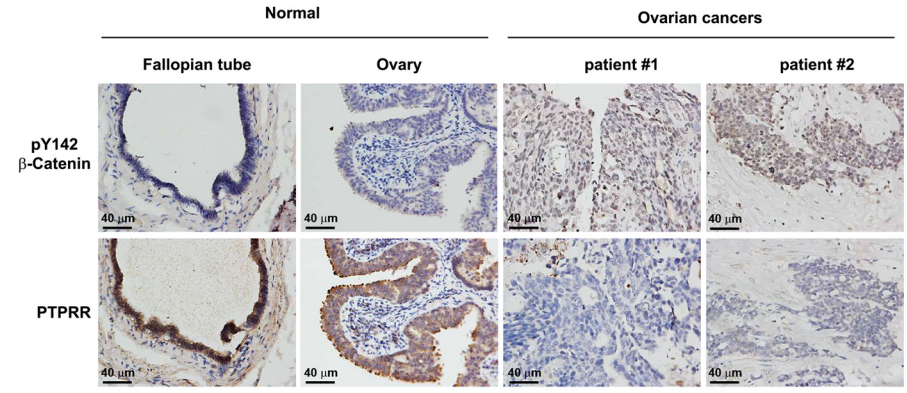

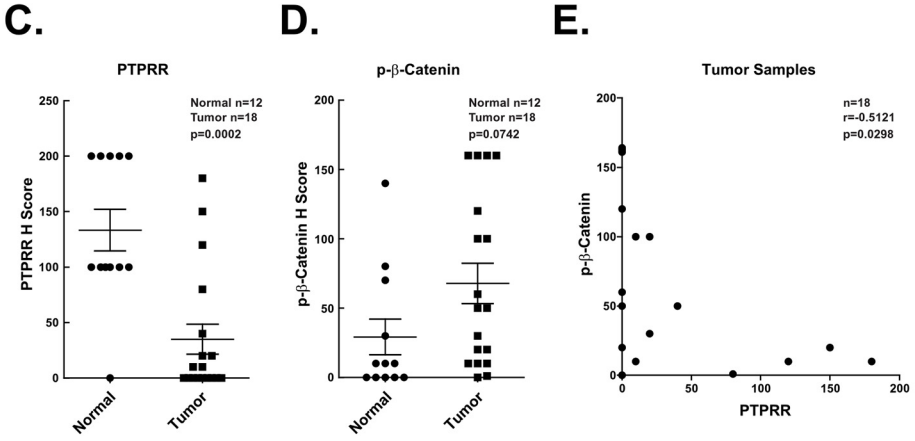

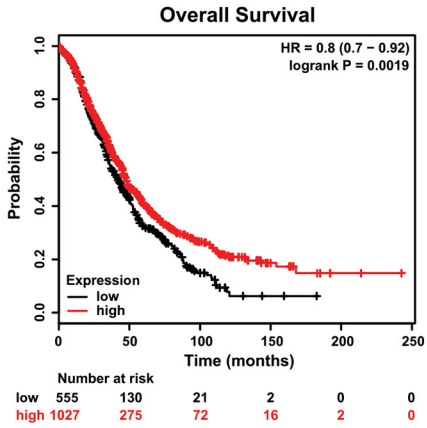

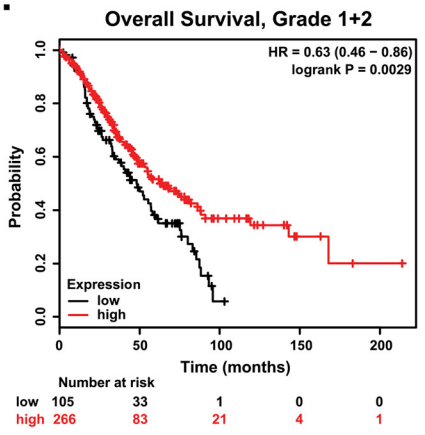

Figure 7. PTPRR was significantly underexpressed in ovarian cancers, and its down-regulation was inversely correlated with prognosis. *A*, representative tissue microarray cores showing diminished expression of PTPRR in malignant ovarian carcinoma sections compared with normal ovary. Data were taken from the Human Protein Atlas. *B*, summary of the immunohistochemistry results for PTPRR protein. *C*, immunohistochemistry staining (pTyr-142 β-catenin and PTPRR) of normal ($n = 12$) and ovarian carcinoma ($n = 18$) samples. Results represent mean ± S.D. (*error bars*). *D*, statistical analysis of PTPRR H score between normal ($n = 12$) and ovarian carcinoma ($n = 18$) samples. Results represent mean ± S.D. *E*, correlation analysis of pTyr-142 β-catenin and PTPRR H score in ovarian carcinoma ($n = 18$) samples. *F*, PTPRR expression was stratified as high *versus* low against median expression. Overall survival within previously published data sets was analyzed using km Plotter (http://kmplot.com/analysis/)[5] (58). *G*, PTPRR expression was stratified as high *versus* low against median expression. Overall survival within patients identified at disease grades 1 and 2 was further analyzed using km Plotter (http://kmplot.com/analysis/)[5] (58).

the different proteins between OVCAR5 cells with PTPRR-WT and PTPRR-DA expression, we calculated the -fold change of LFQ intensity and used a *t* test to calculate the *p* value. -Fold change >2 or <0.5 and a *p* value <0.05 were regarded as significantly different proteins. Then the data were plotted using GraphPad Prism.

Immunoblotting and immunoprecipitation

Cell extracts were prepared in 1% Nonidet P-40 lysis buffer (20 mM Hepes, pH 7.5, 150 mM NaCl, 1% Nonidet P-40, 50 mM NaF, 1 mM Na_3VO_4, 10% glycerol, and protease inhibitor mixture from Roche Applied Science) at 4 °C for 30 min. Total protein concentration was determined using the Bradford

assay. Proteins were resolved by SDS-PAGE and transferred to a nitrocellulose membrane. Membranes were blocked in 5% BSA in TBST (TBS/Tween 20: 20 mM Tris/HCl, pH 7.6, 136 mM NaCl, and 0.1% Tween 20) and incubated at 4 °C overnight with primary antibody. Proteins were detected with horseradish peroxidase– conjugated secondary antibodies (Jackson Laboratory) and ECL (Pierce). The primary antibodies used in this study were as follows: pTyr-142 β-catenin (CP1081, ECM Bioscience) diluted 1:500, β-catenin (CM1181, ECM Bioscience) diluted 1:500, α-catenin (A5635, Abclonal) diluted 1:1,000, lamin B (sc-6216, Santa Cruz Biotechnology, Inc.) diluted 1:500, γ-tubulin (T6557, Sigma) diluted 1:1,000, actin (A2066, Sigma) diluted 1:10,000, GAPDH (NB300-221E, Novus Biologicals) diluted 1:1,000, LEF1 (catalog no. 2230, Cell Signaling Technology) diluted 1:1,000, TCF1 (catalog no. 2203, Cell Signaling Technology) diluted 1:1,000, TCF3 (catalog no. 2883, Cell Signaling Technology) diluted 1:1,000, TCF4 (catalog no. 2569, Cell Signaling Technology) diluted 1:1,000, SFRP1 (catalog no. 3534, Cell Signaling Technology) diluted 1:1,000, pERK1/2 (Thr-202/Tyr-204) (catalog no. 4377, Cell Signaling Technology) diluted 1:1,000, ERK1/2 (catalog no. 4695, Cell Signaling Technology) diluted 1:1,000, PTPN6 (catalog no. 3759, Cell Signaling Technology) diluted 1:1,000, PTPN11 (catalog no. 3397, Cell Signaling Technology) diluted 1:1,000, pTyr-416 Src (catalog no. 2101, Cell Signaling Technology) diluted 1:1000, pTyr-527 Src (catalog no. 2105, Cell Signaling Technology) diluted 1:1,000, Src (catalog no. 2110, Cell Signaling Technology) diluted 1:1,000, E-cadherin (catalog no. 3195, Cell Signaling Technology) diluted 1:1,000, PTPRR (PA5-29243, Invitrogen) diluted 1:1,000, PTPRH (diluted 1:1,000, PA5-31340, Invitrogen), PTPRS (AF3430, R&D Systems) diluted 1:1,000, PTPRU (MAB7475, R&D Systems) diluted 1:1,000, PTPRU (610350, BD Bioscience) diluted 1:1,000, PTPRU (610350, BD Bioscience) diluted 1:1,000, and PTPN22 (H00026191-M01, Abnova) diluted 1:1,000. Primary antibodies, including PTPRM, PTPN2, and PTPRJ, were gifts from Prof. N. K. Tonks (Cold Spring Harbor Laboratory). PTPRK primary antibody was a gift from Prof. A. Ullrich (Max-Planck). PTPN23 primary antibody was a gift from Prof. A Pause (McGill University).

For immunoprecipitation, precleared cell extracts were incubated with the indicated antibody for 4 h in a cold room with rotation followed by 1 h of pulldown by 1:1 Protein A/G-agarose beads. Immunoprecipitates were washed with lysis buffer three times before electrophoresis.

ChIP-PCR

OVCAR5 cells or OVCAR5 cells expressing WT or trapping mutant of PTPRR were cross-linked with 1% formaldehyde for 5 min at room temperature, lysed by SDS lysis buffer, and sonicated to generate DNA fragments with an average size of 500 bp. After preclearing with Protein A/G beads, antibodies against β-catenin (610154, BD Biosciences) or control mouse IgG was added to cell lysate and incubated at 4 °C overnight. DNA cross-linked with β-catenin was pulled down with Protein A/G beads and washed and purified with the MinElute PCR purification kit (catalog no. 28004, Qiagen). Aliquots of CHIP-enriched DNA and whole-cell lysate DNA were subjected to PCR analyses.

qRT-PCR

Total RNAs were prepared as described previously (6, 55) and retrotranscribed into first-strand cDNA using the first-strand synthesis system following the manufacturer's protocol (catalog no. 1708840, Bio-Rad). qRT-PCR was performed using an ABI 7500 sequence detection system (PerkinElmer Life Sciences). Primer sequences are listed in Table S1.

Gene knockdown using shRNAs

Lentivirus-mediated delivery of shRNAs directed against ARID3C and CTNNA1 (α-catenin) were performed as described previously (55). shRNAs were packaged in lentiviral particles by co-transfection with packaging plasmids into HEK-293T cells, and the filtered cell culture supernatant was then used to infect cells. The shRNA sequences are listed in Table S1.

RNA-Seq and bioinformatics analysis

Total RNAs from OVCAR5 cells, OVCAR5 cells expressing WT or trapping mutant of PTPRR as well as xenograft tumors from OVCAR5 cells, or OVCAR5 cells expressing WT or trapping mutant of PTPRR were used for RNA-Seq analysis. We aligned the reads to hg19 using Tophat2, and gene counts were calculated by htseq-count tools.

Animal work

All study protocols involving mice were approved by the institutional animal care and use committee of ShanghaiTech University and conducted in accordance with governmental regulations of China for the care and use of animals.

In the subcutaneous injection model, 1×10^6 OVCAR5 cells or OVCAR5 cells expressing WT or trapping mutant of PTPRR were suspended in 100 μl of 1:1 mixture with Dulbecco's modified Eagle's medium and growth factor-reduced Matrigel (BD Biosciences) and subcutaneously injected into nude mice. All cells were engineered with a luciferase expression cassette. Subcutaneous tumor growth was monitored periodically by injecting 100 μl of 15 mg/kg D-luciferin (PerkinElmer Life Sciences) intraperitoneally and imaging the animal using a Xenogen imager (Xenogen IVIS-200 optical *in vivo* imaging system). Tumor volume (formula: volume = width^2 × length/2; in mm^3) and weight (g) of all subcutaneous tumors were measured.

In the intraperitoneal injection model, 5×10^6 OVCAR5 cells or OVCAR5 cells expressing WT, DA mutant of PTPRR, or SHP1 were suspended in 100 μl of 1:1 1× PBS and into the peritoneum (body cavity) of nude mice at 6 weeks. Mice were analyzed 6 weeks after injection.

Immunohistochemistry staining

Tissues were fixed in 10% buffered formalin for 24 h, followed by a gentle wash and transfer to PBS. Then paraffin-embedded tissues were sectioned to 6-μm-thick, placed on charged glass slides, and stained with hematoxylin and eosin or appropriate immunohistochemical stains. Antigen retrieval was performed by incubating the slides in 0.01 mol/liter citric acid buffer (pH 6.0) at 95 °C for 15 min. Slides were then

allowed to cool to room temperature for 20 min in a citric acid buffer. After the slides were washed with deionized water, they were transferred to TBS (pH 7.4) for 5 min. Slides were counterstained in Mayer's hematoxylin, dehydrated, cleared, and coverslipped. Negative control slides were run without primary antibody. Control slides known to be positive for each antibody were incorporated. Antibodies used in this staining were pTyr-142 and total β-catenin (ECM Bioscience) and PTPRR (Invitrogen).

Sections were first blocked with 5% normal horse serum and 1% BSA (in TBS) for 1 h at room temperature, and then the primary antibodies were diluted, as suggested by the manufacturer, and incubated overnight at 4 °C. Following three 10-min washes with TBS, sections were incubated with biotinylated secondary antibody for 30 min at room temperature and rinsed with TBS three times for 10 min. Finally, the sections were treated with diaminobenzidine for 3 min and rinsed with distilled water to end the reaction, mounted on gelatin-coated slides, air-dried, dehydrated with 70–100% alcohol, cleared with xylene, and coverslipped for microscopic observation. After examination of all immunohistochemical and special stains, stained slides were digitally scanned using the Aperio ScanScope software. Staining strength was classified into three levels.

H score was used for statistical analysis and calculated as positive staining percentage multiplied by staining strength (56). Briefly, all specimens were evaluated in a blinded setting to evaluate staining intensity of analyzed cells (on a scale of 0–3) and the fraction of cells staining at each intensity. We adopted a scoring system to calculate the score of intensity times the percentage of the stained tumor cells. For sections with analyzable tumor cells, staining intensity was scored in four categories: no staining (0), weak staining (1+), intermediate staining (2+, between 1+ and 3+), and strong staining (3+). The percentages of tumor cells showing the different staining intensities were assessed visually. We used the prospectively collected IHC data to generate IHC scores on a continuous scale of 0–300. By integration of the data relating to the intensity and frequency of staining, the IHC score was calculated with the formula, 1 × (percentage of cells staining weakly (1+)) + 2 × (percentage of cells staining moderately (2+)) + 3 × (percentage of cells staining strongly (3+)).

Author contributions—Y. W. data curation; Y. W., J. Z., Z. W., and S. C. investigation; Y. W. and G. F. writing-original draft; Y. W., M. Z., and G. F. project administration; J. C. and D. L. resources; W. L., Y. Z., L. H., L. Z., and Y. Y. formal analysis; P. H. methodology; M. Z., Y. Y., D. L., and G. F. supervision; G. F. funding acquisition.

Acknowledgments—We thank Prof. Nicholas K. Tonks (Cold Spring Harbor Laboratory) for reagent support for protein tyrosine phosphatase research in this study. We also thank Dr. Haopeng Wang (ShanghaiTech University) for helpful comments in the preparation of the manuscript.

References

1. Torre, L. A., Trabert, B., DeSantis, C. E., Miller, K. D., Samimi, G., Runowicz, C. D., Gaudet, M. M., Jemal, A., and Siegel, R. L. (2018) Ovarian cancer statistics, 2018. *CA Cancer J. Clin.* **68,** 284–296 CrossRef Medline
2. Siegel, R. L., Miller, K. D., and Jemal, A. (2018) Cancer statistics, 2018. *CA Cancer J. Clin.* **68,** 7–30 CrossRef Medline
3. McGuire, W. P. (2009) Maintenance therapy for ovarian cancer: of Helsinki and Hippocrates. *J. Clin. Oncol.* **27,** 4633–4634 CrossRef Medline
4. Binaschi, M., Simonelli, C., Goso, C., Bigioni, M., and Maggi, C. A. (2011) Maintenance therapy in ovarian cancer: molecular basis and therapeutic approach. *Exp. Ther. Med.* **2,** 173–180 CrossRef Medline
5. Coleman, M. P., Forman, D., Bryant, H., Butler, J., Rachet, B., Maringe, C., Nur, U., Tracey, E., Coory, M., Hatcher, J., McGahan, C. E., Turner, D., Marrett, L., Gjerstorff, M. L., Johannesen, T. B., *et al.* (2011) Cancer survival in Australia, Canada, Denmark, Norway, Sweden, and the UK, 1995–2007 (the International Cancer Benchmarking Partnership): an analysis of population-based cancer registry data. *Lancet* **377,** 127–138 CrossRef Medline
6. Reya, T., and Clevers, H. (2005) Wnt signalling in stem cells and cancer. *Nature* **434,** 843–850 CrossRef Medline
7. Clevers, H. (2006) Wnt/β-catenin signaling in development and disease. *Cell* **127,** 469–480 CrossRef Medline
8. Wang, H. X., Tekpetey, F. R., and Kidder, G. M. (2009) Identification of WNT/β-CATENIN signaling pathway components in human cumulus cells. *Mol. Hum. Reprod.* **15,** 11–17 CrossRef Medline
9. Oksjoki, S., Söderström, M., Inki, P., Vuorio, E., and Anttila, L. (2005) Molecular profiling of polycystic ovaries for markers of cell invasion and matrix turnover. *Fertil. Steril.* **83,** 937–944 CrossRef Medline
10. Boyer, A., Goff, A. K., and Boerboom, D. (2010) WNT signaling in ovarian follicle biology and tumorigenesis. *Trends Endocrinol. Metab.* **21,** 25–32 CrossRef Medline
11. Wu, R., Zhai, Y., Fearon, E. R., and Cho, K. R. (2001) Diverse mechanisms of β-catenin deregulation in ovarian endometrioid adenocarcinomas. *Cancer Res.* **61,** 8247–8255 Medline
12. Dubeau, L. (2008) The cell of origin of ovarian epithelial tumours. *Lancet Oncol.* **9,** 1191–1197 CrossRef Medline
13. McConechy, M. K., Ding, J., Senz, J., Yang, W., Melnyk, N., Tone, A. A., Prentice, L. M., Wiegand, K. C., McAlpine, J. N., Shah, S. P., Lee, C. H., Goodfellow, P. J., Gilks, C. B., and Huntsman, D. G. (2014) Ovarian and endometrial endometrioid carcinomas have distinct CTNNB1 and PTEN mutation profiles. *Mod. Pathol.* **27,** 128–134 CrossRef Medline
14. Saegusa, M., and Okayasu, I. (2001) Frequent nuclear β-catenin accumulation and associated mutations in endometrioid-type endometrial and ovarian carcinomas with squamous differentiation. *J. Pathol.* **194,** 59–67 CrossRef Medline
15. Rask, K., Nilsson, A., Brännström, M., Carlsson, P., Hellberg, P., Janson, P. O., Hedin, L., and Sundfeldt, K. (2003) Wnt-signalling pathway in ovarian epithelial tumours: increased expression of β-catenin and GSK3β. *Br. J. Cancer* **89,** 1298–1304 CrossRef Medline
16. Takebe, N., Harris, P. J., Warren, R. Q., and Ivy, S. P. (2011) Targeting cancer stem cells by inhibiting Wnt, Notch, and Hedgehog pathways. *Nat. Rev. Clin. Oncol.* **8,** 97–106 CrossRef Medline
17. Barbolina, M. V., Burkhalter, R. J., and Stack, M. S. (2011) Diverse mechanisms for activation of Wnt signalling in the ovarian tumour microenvironment. *Biochem. J.* **437,** 1–12 CrossRef Medline
18. Brembeck, F. H., Rosário, M., and Birchmeier, W. (2006) Balancing cell adhesion and Wnt signaling, the key role of β-catenin. *Curr. Opin. Genet. Dev.* **16,** 51–59 CrossRef Medline
19. Roura, S., Miravet, S., Piedra, J., García de Herreros, A., and Duñach, M. (1999) Regulation of E-cadherin/catenin association by tyrosine phosphorylation. *J. Biol. Chem.* **274,** 36734–36740 CrossRef Medline
20. Piedra, J., Miravet, S., Castaño, J., Pálmer, H. G., Heisterkamp, N., García de Herreros, A., and Duñach, M. (2003) p120 catenin-associated Fer and Fyn tyrosine kinases regulate β-catenin Tyr-142 phosphorylation and β-catenin-α-catenin interaction. *Mol. Cell. Biol.* **23,** 2287–2297 CrossRef Medline
21. Aberle, H., Schwartz, H., Hoschuetzky, H., and Kemler, R. (1996) Single amino acid substitutions in proteins of the armadillo gene family abolish their binding to α-catenin. *J. Biol. Chem.* **271,** 1520–1526 CrossRef Medline

22. Pokutta, S., and Weis, W. I. (2000) Structure of the dimerization and β-catenin-binding region of α-catenin. *Mol. Cell* **5,** 533–543 CrossRef Medline
23. Mishra, J., Das, J. K., Kumar, N. (2017) Janus kinase 3 regulates adherens junctions and epithelial mesenchymal transition through β-catenin. *J. Biol. Chem.* **292,** 16406–16419 CrossRef Medline
24. Brembeck, F. H., Schwarz-Romond, T., Bakkers, J., Wilhelm, S., Hammerschmidt, M., and Birchmeier, W. (2004) Essential role of BCL9–2 in the switch between β-catenin's adhesive and transcriptional functions. *Genes Dev.* **18,** 2225–2230 CrossRef Medline
25. Hoffmans, R., and Basler, K. (2004) Identification and *in vivo* role of the Armadillo-Legless interaction. *Development* **131,** 4393–4400 CrossRef Medline
26. Arend, R. C., Londoño-Joshi, A. I., Straughn, J. M., Jr., and Buchsbaum, D. J. (2013) The Wnt/β-catenin pathway in ovarian cancer: a review. *Gynecol. Oncol.* **131,** 772–779 CrossRef Medline
27. Tsao, S. W., Mok, S. C., Fey, E. G., Fletcher, J. A., Wan, T. S., Chew, E. C., Muto, M. G., Knapp, R. C., and Berkowitz, R. S. (1995) Characterization of human ovarian surface epithelial cells immortalized by human papilloma viral oncogenes (HPV-E6E7 ORFs). *Exp. Cell Res.* **218,** 499–507 CrossRef Medline
28. Xu, G., Craig, A. W., Greer, P., Miller, M., Anastasiadis, P. Z., Lilien, J., and Balsamo, J. (2004) Continuous association of cadherin with β-catenin requires the non-receptor tyrosine-kinase Fer. *J. Cell Sci.* **117,** 3207–3219 CrossRef Medline
29. Fan, G., Zhang, S., Gao, Y., Greer, P. A., and Tonks, N. K. (2016) HGF-independent regulation of MET and GAB1 by nonreceptor tyrosine kinase FER potentiates metastasis in ovarian cancer. *Genes Dev.* **30,** 1542–1557 CrossRef Medline
30. Lilien, J., and Balsamo, J. (2005) The regulation of cadherin-mediated adhesion by tyrosine phosphorylation/dephosphorylation of β-catenin. *Curr. Opin. Cell Biol.* **17,** 459–465 CrossRef Medline
31. Zhang, S., Fan, G., Hao, Y., Hammell, M., Wilkinson, J. E., and Tonks, N. K. (2017) Suppression of protein tyrosine phosphatase N23 predisposes to breast tumorigenesis via activation of FYN kinase. *Genes Dev.* **31,** 1939–1957 CrossRef Medline
32. Blanco-Aparicio, C., Torres, J., and Pulido, R. (1999) A novel regulatory mechanism of MAP kinases activation and nuclear translocation mediated by PKA and the PTP-SL tyrosine phosphatase. *J. Cell Biol.* **147,** 1129–1136 CrossRef Medline
33. Liu, Q., Zheng, J., Sun, W., Huo, Y., Zhang, L., Hao, P., Wang, H., and Zhuang, M. (2018) A proximity-tagging system to identify membrane protein-protein interactions. *Nat. Methods* **15,** 715–722 CrossRef Medline
34. Pedrosa, E., Shah, A., Tenore, C., Capogna, M., Villa, C., Guo, X., Zheng, D., and Lachman, H. M. (2010) β-Catenin promoter ChIP-chip reveals potential schizophrenia and bipolar disorder gene network. *J. Neurogenet.* **24,** 182–193 CrossRef Medline
35. Clevers, H., and Nusse, R. (2012) Wnt/β-catenin signaling and disease. *Cell* **149,** 1192–1205 CrossRef Medline
36. Lammi, L., Arte, S., Somer, M., Jarvinen, H., Lahermo, P., Thesleff, I., Pirinen, S., and Nieminen, P. (2004) Mutations in AXIN2 cause familial tooth agenesis and predispose to colorectal cancer. *Am. J. Hum. Genet.* **74,** 1043–1050 CrossRef Medline
37. Morin, P. J., Sparks, A. B., Korinek, V., Barker, N., Clevers, H., Vogelstein, B., and Kinzler, K. W. (1997) Activation of β-catenin-Tcf signaling in colon cancer by mutations in β-catenin or APC. *Science* **275,** 1787–1790 CrossRef Medline
38. Assié, G., Letouzé, E., Fassnacht, M., Jouinot, A., Luscap, W., Barreau, O., Omeiri, H., Rodriguez, S., Perlemoine, K., René-Corail, F., Elarouci, N., Sbiera, S., Kroiss, M., Allolio, B., Waldmann, J., *et al.* (2014) Integrated genomic characterization of adrenocortical carcinoma. *Nat. Genet.* **46,** 607–612 CrossRef Medline
39. Su, P. H., Lin, Y. W., Huang, R. L., Liao, Y. P., Lee, H. Y., Wang, H. C., Chao, T. K., Chen, C. K., Chan, M. W., Chu, T. Y., Yu, M. H., and Lai, H. C. (2013) Epigenetic silencing of PTPRR activates MAPK signaling, promotes metastasis and serves as a biomarker of invasive cervical cancer. *Oncogene* **32,** 15–26 CrossRef Medline
40. Min, J. W., Koh, Y., Kim, D. Y., Kim, H. L., Han, J. A., Jung, Y. J., Yoon, S. S., and Choi, S. S. (2018) Identification of novel functional variants of SIN3A and SRSF1 among somatic variants in acute myeloid leukemia patients. *Mol. Cells* **41,** 465–475 CrossRef Medline
41. Duś-Szachniewicz, K., Woźniak, M., Nelke, K., Gamian, E., Gerber, H., and Ziółkowski, P. (2015) Protein tyrosine phosphatase receptor R and Z1 expression as independent prognostic indicators in oral squamous cell carcinoma. *Head Neck* **37,** 1816–1822 CrossRef Medline
42. Munkley, J., Lafferty, N. P., Kalna, G., Robson, C. N., Leung, H. Y., Rajan, P., and Elliott, D. J. (2015) Androgen-regulation of the protein tyrosine phosphatase PTPRR activates ERK1/2 signalling in prostate cancer cells. *BMC Cancer* **15,** 9 CrossRef Medline
43. Shen, S., Gui, T., and Ma, C. (2017) Identification of molecular biomarkers for pancreatic cancer with mRMR shortest path method. *Oncotarget* **8,** 41432–41439 CrossRef Medline
44. Li, X., Liu, Z., Li, W., Sun, N., Xu, Y., Xie, Z., and Zhang, K. (2016) PTPRR regulates ERK dephosphorylation in depression mice model. *J. Affect. Disord.* **193,** 233–241 CrossRef Medline
45. Wilsker, D., Probst, L., Wain, H. M., Maltais, L., Tucker, P. W., and Moran, E. (2005) Nomenclature of the ARID family of DNA-binding proteins. *Genomics* **86,** 242–251 CrossRef Medline
46. Tidwell, J. A., Schmidt, C., Heaton, P., Wilson, V., and Tucker, P. W. (2011) Characterization of a new ARID family transcription factor (Brightlike/ARID3C) that co-activates Bright/ARID3A-mediated immunoglobulin gene transcription. *Mol. Immunol.* **49,** 260–272 CrossRef Medline
47. Kim, S., Zhang, Z., Upchurch, S., Isern, N., and Chen, Y. (2004) Structure and DNA-binding sites of the SWI1 AT-rich interaction domain (ARID) suggest determinants for sequence-specific DNA recognition. *J. Biol. Chem.* **279,** 16670–16676 CrossRef Medline
48. Tu, M. J., Ho, P. Y., Zhang, Q. Y., Jian, C., Qiu, J. X., Kim, E. J., Bold, R. J., Gonzalez, F. J., Bi, H., and Yu, A. M. (2019) Bioengineered miRNA-1291 prodrug therapy in pancreatic cancer cells and patient-derived xenograft mouse models. *Cancer Lett.* **442,** 82–90 CrossRef Medline
49. Nakahara, S., Fukushima, S., Yamashita, J., Kubo, Y., Tokuzumi, A., Miyashita, A., Harada, M., Nakamura, K., Jinnin, M., and Ihn, H. (2017) AT-rich interaction domain-containing protein 3B is a new tumour marker for melanoma. *Acta Derm. Venereol.* **97,** 112–114 CrossRef Medline
50. Chien, C. S., Wang, M. L., Chu, P. Y., Chang, Y. L., Liu, W. H., Yu, C. C., Lan, Y. T., Huang, P. I., Lee, Y. Y., Chen, Y. W., Lo, W. L., and Chiou, S. H. (2015) Lin28B/Let-7 regulates expression of Oct4 and Sox2 and reprograms oral squamous cell carcinoma cells to a stem-like state. *Cancer Res.* **75,** 2553–2565 CrossRef Medline
51. Cowden Dahl, K. D., Dahl, R., Kruichak, J. N., and Hudson, L. G. (2009) The epidermal growth factor receptor responsive miR-125a represses mesenchymal morphology in ovarian cancer cells. *Neoplasia* **11,** 1208–1215 CrossRef Medline
52. Bobbs, A., Gellerman, K., Hallas, W. M., Joseph, S., Yang, C., Kurkewich, J., and Cowden Dahl, K. D. (2015) ARID3B directly regulates ovarian cancer promoting genes. *PLoS One* **10,** e0131961 CrossRef Medline
53. Roy, L., Samyesudhas, S. J., Carrasco, M., Li, J., Joseph, S., Dahl, R., and Cowden Dahl, K. D. (2014) ARID3B increases ovarian tumor burden and is associated with a cancer stem cell gene signature. *Oncotarget* **5,** 8355–8366 CrossRef Medline
54. Lin, G., Aranda, V., Muthuswamy, S. K., and Tonks, N. K. (2011) Identification of PTPN23 as a novel regulator of cell invasion in mammary epithelial cells from a loss-of-function screen of the "PTP-ome". *Genes Dev.* **25,** 1412–1425 CrossRef Medline
55. Gao, Y., Xiao, Q., Ma, H., Li, L., Liu, J., Feng, Y., Fang, Z., Wu, J., Han, X., Zhang, J., Sun, Y., Wu, G., Padera, R., Chen, H., Wong, K., *et al.* (2010) LKB1 inhibits lung cancer progression through lysyl oxidase and extracellular matrix remodeling. *Proc. Natl. Acad. Sci. U.S.A.* **107,** 18892–18897 CrossRef Medline
56. Ren, S., Su, C., Wang, Z., Li, J., Fan, L., Li, B., Li, X., Zhao, C., Wu, C., Hou, L., He, Y., Gao, G., Chen, X., Ren, J., Li, A., Xu, G., Zhou, X., Zhou, C., and Schmid-Bindert, G. (2014) Epithelial phenotype as a predictive marker for

response to EGFR-TKIs in non-small cell lung cancer patients with wild-type EGFR. *Int. J. Cancer* **135,** 2962–2971 CrossRef Medline

57. Perez-Riverol, Y., Csordas, A., Bai, J., Bernal-Llinares, M., Hewapathirana, S., Kundu, D. J., Inuganti, A., Griss, J., Mayer, G., Eisenacher, M., Pérez, E., Uszkoreit, J., Pfeuffer, J., Sachsenberg, T., Yilmaz, S., *et al.* (2019) The PRIDE database and related tools and resources in 2019: improving support for quantification data. *Nucleic Acids Res.* **47,** D442–D450 CrossRef Medline
58. Nagy, Á., Lánczky, A., Menyhárt, O., and Gyrffy, B. (2018) Validation of miRNA prognostic power in hepatocellular carcinoma using expression data of independent datasets. *Sci. Rep.* **8,** 9227 CrossRef Medline
59. Olson A., Sheth, N., Lee, J. S., Hannon, G., and Sachidanandam, R. (2006) RNAi Codex: a portal/database for short-hairpin RNA (shRNA) gene-silencing constructs. *Nucleic Acids Res.* **34,** D153–D157 CrossRef Medline